Title: Engineered Immunogens to Elicit Antibodies Against Conserved Coronavirus Epitopes

Authors: Brenda Kapingidza[1,2,#], Daniel J. Marston[1,2,#], Caitlin Harris[1,2], Daniel Wrapp[1,2], Kaitlyn Winters[1,2], Dieter Mielke[3,4], Lu Xiaozhi[1,2], Qi Yin[1,2], Andrew Foulger[1,2], Rob Parks[1,2], Maggie Barr[1,2], Amanda Newman[1,2], Alexandra Schäfer[5], Amanda Eaton[3], Justine Mae Flores[1,2], Austin Harner[1,2], Nicholas J Cantazaro Jr.[5], Michael L Mallory[5], Melissa D Mattocks[5], Christopher Beverly[1,2], Brianna Rhodes[1,2], Katayoun Mansouri[1], Elizabeth Van Itallie[1,2], Pranay Vure[1,2], Brooke Manness[3], Taylor Keyes[3], Sherry Stanfield-Oakley[3], Christopher W. Woods[1,2,7], Elizabeth A. Petzold[7], Emmanuel B Walter[1,8], Kevin Wiehe[1,2], Robert J. Edwards[1,2], David Montefiori[3], Guido Ferrari[1,3,4,6], Ralph Baric[5], Derek W. Cain[1,2], Kevin O. Saunders[1,3,6,9], Barton F. Haynes[1,2,9], Mihai L. Azoitei[1,2,*]

Affiliations:

[1]Duke Human Vaccine Institute, Duke University, Durham, NC

[2]Department of Medicine, Duke University, Durham, NC

[3]Department of Surgery, Duke University, Durham, NC

[4]Center for Human Systems Immunology, Duke University, Durham, NC, USA;

[5]Department of Epidemiology, University of North Carolina at Chapel Hill, Chapel Hill, NC

[6]Department of Molecular Genetics and Microbiology, Duke University, Durham, NC

[7]Center for Infectious Diseases and Diagnostic Innovation, Duke University Medical Center, Durham, NC

[8]Department of Pediatrics, Duke University, Durham NC

[9]Department of Immunology, Duke University, Durham, NC

[#]These authors contributed equally to this work.

* Corresponding author. Email: mihai.azoitei@duke.edu

Key Words: SARS-CoV-2, vaccine, epitope-scaffolds, stem helix, pan-coronavirus vaccine

Abstract:

Immune responses to SARS-CoV-2 primarily target the receptor binding domain of the spike protein, which continually mutates to escape acquired immunity. Other regions in the spike S2 subunit, such as the stem helix and the segment encompassing residues 815-823 adjacent to the fusion peptide, are highly conserved across sarbecoviruses and are recognized by broadly reactive antibodies, providing hope that vaccines targeting these epitopes could offer protection against both current and emergent viruses. Here we employed computational modeling to design scaffolded immunogens that display the spike 815-823 peptide and the stem helix epitopes without the distracting and immunodominant RBD. These engineered proteins bound with high affinity and specificity to the mature and germline versions of previously identified broadly protective human antibodies. Epitope scaffolds interacted with both sera and isolated monoclonal antibodies with broadly reactivity from individuals with pre-existing SARS-CoV-2 immunity. When used as immunogens, epitope scaffolds elicited sera with broad betacoronavirus reactivity and protected as “boosts” against live virus challenge in mice, illustrating their potential as components of a future pancoronavirus vaccine.

Main Text:

The majority of immune responses elicited against SARS-CoV-2, by either natural infection, vaccination or a combination of both, are focused on the receptor binding domain (RBD)[1-4]. However, deep scanning mutagenesis studies[5] and the emergence of novel variants that evade pre-existing immunity have revealed the plastic nature of the RBD[2,6], suggesting that next-generation coronavirus vaccines designed to protect against both current and emergent CoVs will need to induce antibodies against CoV spike regions beyond the RBD.

Two regions in the S2 subunit of the SARS-CoV-2 spike, the segment encompassing residues 815-823 adjacent to the fusion peptide and the stem helix domain (residues 1145-1156), show high conservation across diverse coronaviruses. Isolated antibodies that target these sites cross-react with both alpha and beta human coronaviruses, and protect by either neutralization, Fc receptor mediated mechanisms or both[7-10]. For example, antibodies DH1058, DH1294, VN01H1, Cov44-79, and Cov44-62, bind to an epitope located around SARS-CoV-2 spike residues 815-823 and recognize all seven human CoVs[7,8,11,12]. Antibodies against the stem helix region, such as S2P6 and CC40.8[9,10,13,14], bound spike glycoproteins representative of all sarbecovirus clades, and protected against viral challenge by inhibiting S-mediated membrane fusion. Despite their attractiveness as vaccine targets, humoral responses against the stem helix or the spike 815-823 epitopes are not robustly induced by existing vaccines or by natural infection[7-10]. This is likely due to a combination of factors, including the occlusion of these epitopes on the pre-fusion spike, requiring ACE2 binding for exposure[8], as well as the presence of the prominently displayed, immunodominant RBD domain. Given their ability to recognize diverse coronaviruses, immunogens that induce strong responses against the spike 815-823 region and the stem helix could be a key component of a future “pan-coronavirus” vaccine offering broad protection against both currently circulating and emergent coronaviruses.

70 For the design of immunogens that expose occluded epitopes in novel molecular contexts,
71 we and others previously described the development of “epitope scaffold” proteins[15-17]. These
72 molecules are engineered by transplanting the structure of the antibody-bound epitopes from viral
73 molecules onto unrelated protein scaffolds. Unlike peptide-based immunogens that can sample
74 diverse epitope conformations, epitope scaffolds are meant to present only the antibody-bound
75 conformation of the target epitope on their surface, which typically leads to higher antibody affinity
76 and the elicitation of antibodies specific for the structure of the target epitope[18,19]. Here, we applied
77 epitope grafting to design stem helix or spike 815-823 epitope scaffolds that strongly interact with
78 broadly cross-reactive antibodies against these regions of spike. These antigens were used to
79 isolate diverse antibodies with broad reactivity against these conserved epitopes from subjects
80 with pre-existing SARS-CoV-2 immunity. When used as immunogens in mice, epitope scaffolds
81 elicited sera with broad betacoronavirus reactivity. In a viral challenge model, boosting responses
82 induced by spike mRNA with stem helix epitope scaffolds offered protection against a pre-
83 emergent coronavirus, thus illustrating the potential of the immunogens engineered here as next-
84 generation vaccine candidates to preferentially boost antibodies that may protect against existing
85 and emerging coronaviruses.

86

87 ## Results

88 **Design of epitope scaffolds that bind broadly cross-reactive antibodies against the**
89 **spike 815-823 epitope.**

90 The region containing residues 815-823 of the SARS-CoV-2 spike, thereafter referred to
91 as spike$^{815-823}$, was initially thought to be part of the fusion peptide domain. However, recent
92 structural analysis of the post-fusion spike in a lipid environment revealed that the actual fusion

93 peptide is located upstream of this region (residues 867-909). While the functional role of the
94 spike$^{815-823}$ region remains to be determined, multiple broadly protective antibodies, such as
95 DH1058, DH1294, VN01H1, Cov44-79, and Cov44-62 target this site, with key contacts made
96 with virus residues R815, E819 and F823 (**Figure 1a**, **Supp. Fig. 1**)[7,8,11,12]. These residues are
97 occluded in the structure of the prefusion SARS-CoV-2 spike, likely limiting their immune
98 recognition (**Figure 1a**). To improve the accessibility and immune recognition of this epitope, we
99 developed spike$^{815-823}$ epitope scaffolds (ES) using "side chain" grafting computational methods
100 that we and others previously described (**Supp. Fig. 2**)[15-17]. A large library (~10,000) of small
101 monomeric scaffolding proteins was queried computationally to identify proteins with exposed
102 backbone regions that closely matched (<0.5Å backbone RMSD) the structure of the spike$^{815-823}$
103 epitope (**Supp. Fig. 2**). In regions with high structural mimicry to the DH1058-bound epitope, the
104 epitope sequence replaced that of the parent scaffold and additional mutations were introduced
105 to accommodate the grafted sequence (**Supp. Fig. 2**).

106 Fifteen engineered spike$^{815-823}$ epitope scaffolds were expressed recombinantly (**Figure**
107 **1b** for representative designs), and six of them produced soluble and stable proteins that bound
108 DH1058 mAb by ELISA (**Supp. Fig. 3**, **Supp. Table 1**). Equilibrium dissociation constants for
109 mAbs DH1058 and DH1294 were determined by surface plasmon resonance (SPR) for the
110 designs that showed tight binding by ELISA (**Figure 1c; Supp. Fig. 4**). FP-2, FP-10, and FP-15
111 bound to DH1058 with picomolar affinities and to DH1294 with K_Ds of 1221nM, 0.1nM and 219nM
112 respectively. These values compare favorably with measured affinities of the full-length WA-2
113 spike to DH1058 and DH1294 mAbs (1.4nM and 25nM respectively). To probe the breadth of
114 their recognition, the binding of spike$^{815-823}$ epitope scaffolds was measured against antibodies
115 VN01H1, C77G12, VP12E7, COV44-79, and COV44-62[7,8], which were not explicitly considered
116 at the design stage (**Figure 1d; Supp. Fig. 5a**). Five designs bound at least 6 out of the 7
117 antibodies tested, with FP-12 and FP-15 binding all of them tighter than spike. In addition to the

118 mature antibodies, binding was also measured to their inferred unmutated common ancestors
119 (UCAs) or germline-reverted forms (iGLs). Spike only showed measurable binding to the DH1058
120 UCA, while FP-12 and FP-2 were bound by DH1058 UCA, DH1294 UCA and VP12E7 iGL (**Figure**
121 **1d; Supp. Fig. 5b**). Taken together, these data show that the engineered FP epitope scaffolds
122 have broad recognition of genetically diverse FP antibodies and their precursors.

123 DH1058 mAb bound three spike$^{815\text{-}823}$ epitope scaffolds with affinities 10-fold higher than
124 that of spike. To ensure that these affinity gains were primarily mediated by the grafted epitope
125 residues and not by contacts between the scaffold and the antibody that are not present in the
126 native DH1058-epitope complex, interface hotspot residues corresponding to SARS-CoV-2 spike
127 amino acids R815, E819, and F823 were mutated to alanine in designs FP-2, FP-10, and FP-15.
128 Each of the three alanine substitutions eliminated DH1058 mAb binding to a synthetic peptide
129 encompassing the spike$^{815\text{-}823}$ epitope, and to designs FP-2 and FP-10, demonstrating that the
130 grafted epitope is the major site of antibody interaction (**Figure 1e**). Two of the three substitutions
131 similarly eliminated DH1058 binding to FP-15, with the F823A equivalent retaining some low-level
132 antibody binding (**Figure 1e**).

133 To further confirm binding specificity and to validate the computational design process, a
134 high resolution (2.2Å) crystal structure of FP-15 in complex with DH1058 mAb was solved (**Figure**
135 **1f, Supp. Table 2**). The experimentally determined structure was in close agreement with that of
136 the computationally generated antibody-ES complex, both overall and over the epitope scaffold
137 only (backbone RMSD <1Å). The epitope conformation engaged by DH1058 on FP-15 was
138 essentially identical to that induced by the antibody on the spike$^{815\text{-}823}$ peptide (backbone
139 RMSD=0.3Å)[11], confirming that the antibody interacts with the epitope presented by the ES in the
140 same manner it binds to its natural target.

141 **Design of epitope scaffolds to engage S2P6-like antibodies against the stem helix**
142 **region of the CoV spike.**

143 Next, we engineered epitope scaffolds to engage antibodies against the stem helix region
144 of the CoV spike. Antibodies such as S2P6, DH1057.1, and CC40.8[9,10,20] bind to an epitope
145 located between residues 1144 and 1158, which is almost completely occluded by the
146 trimerization interface in the pre-fusion spike structure (**Figure 2a**)[9,10,20]. While both CC40.8 and
147 S2P6 target the same spike region and make critical contacts with residues Phe1148 and
148 Phe1156, CC40.8 makes additional interactions with Leu1145 and induces a more extended
149 epitope conformation upon binding (**Figure 2a**)[10]. Because the CC40.8 epitope is longer and
150 includes the S2P6 epitope, we first attempted to engineer epitope scaffolds that display the
151 antibody-bound conformation of the CC40.8 epitope, with the expectation that these molecules
152 would also be capable of binding to S2P6-class antibodies. However, the "side chain" grafting
153 protocol used for FP epitope scaffolds above, did not identify any candidate scaffolds with
154 exposed backbones similar to that of the CC40.8 epitope, likely due to the unusual conformation
155 of this epitope that adopts a distorted alpha-helical shape near the N-terminus (**Figure 2a**). In
156 contrast, multiple candidate epitope scaffolds that displayed the S2P6-bound conformation of the
157 epitope segment 1148-1156 were successfully designed computationally using side chain
158 grafting. This was possible because the S2P6 epitope adopts a canonical alpha-helical structure,
159 with most of the antibody contacting residues contained within three helical turns (**Figure 2a**).

160 Fifteen S2P6-targeted designs, named S2hlx-1 to 15, were chosen for recombinant
161 production in *E. coli* (**Figure 2a** for representative designs; **Supp. Table 1**) and seven yielded
162 soluble protein. In an initial ELISA screen, all seven designs bound both S2P6 and DH1057.1
163 mAbs comparable to or better than a synthesized SARS-CoV-2 stem helix peptide (residues
164 1147-1161). As expected, neither this peptide nor the epitope scaffolds bound CC40.8 mAb due
165 to the lack of epitope residue L1145 (**Supp. Fig. 6**). Stem helix epitope scaffolds had measured

166 equilibrium dissociation constants between 0.2nM and 83nM for S2P6 mAb and between 0.6nM
167 and 4.5uM for DH1057.1 mAb. In the same assay, the equilibrium dissociation constants of spike
168 for S2P6 and DH1057.1 were 0.4nM and 11.5nM respectively (**Figure 2b, c; Supp. Fig. 7 and**
169 **8)**. The designs with the highest affinities, S2hlx-7 and S2hlx-15, had similar binding of S2P6 to
170 that of spike and bound DH1057.1 >10-fold better, thus demonstrating the successful
171 transplantation of the target epitope onto the scaffolds.

172 The binding specificity of S2hlx-4, S2hlx-7 and S2hlx-15 was confirmed by mutating
173 epitope residues equivalent to spike Phe1148, Leu1152 and Phe1156. Alanine mutations limited
174 the binding to both S2P6 and DH1057.1 mAbs in S2hlx-4 and -15 to a similar extent to what as
175 observed for synthesized stem helix peptides (**Figure 2d**)[9]. For S2hlx-7, the individual epitope
176 mutations greatly decreased DH1057.1 mAb interactions but had almost no effect on S2P6 mAb
177 recognition. However, an S2hlx-7 variant that contained alanine substitutions at all three epitope
178 positions completely abrogated binding, thus confirming that antibody interactions were mediated
179 by the grafted epitope residues. In addition, none of the parent scaffolds these designs were
180 based on showed binding to S2P6 or DH1057.1, further demonstrating epitope specificity (**Supp.**
181 **Fig. 9**).

182 High resolution (1.9Å) structural determination by x-ray crystallography of the S2hlx-
183 7/DH1057.1 complex revealed for the first time the structure and interaction mode of the
184 DH1057.1 antibody with the stem helix epitope. DH1057.1 engaged the epitope at the same angle
185 as S2P6 mAb and similarly interacted with residues Phe1148, Leu1152, and Phe1156 (SARS-
186 CoV-2 spike numbering) (**Figure 2e**), as predicted by the alanine mutagenesis (**Figure 2d**). Unlike
187 S2P6, DH1057.1 interacts with residue K1149 through hydrogen bonds mediated by heavy chain
188 residues Asp95 and Asp100C (**Figure 2e**). The structure of S2hlx-7 in the complex was closely
189 aligned with that of the computational model both overall (backbone RMSD=0.5Å) and, most
190 importantly, over the grafted epitope region (backbone RMSD=0.25Å) (**Figure 2f**). The epitope

191 conformation displayed on S2hlx-7 closely matched that of the antibody-bound S2P6 epitope and
192 that of the corresponding region on the prefusion spike (backbone RMSD<0.2Å, **Figure 2f**). These
193 data validated the computational design of antigens that have high affinity and specificity for
194 S2P6-like mAbs by mimicking the conformation of their epitope on native spikes.

195 **Design of epitope scaffolds that engage stem helix antibodies with different**
196 **specificities.**

197 Given the failure of side chain grafting to produce epitope scaffolds that engage the
198 CC40.8 mAb, we employed an alternative design technique, termed backbone grafting. Here,
199 rather than transplanting only the epitope-specific residues onto a preexisting scaffold backbone
200 which is otherwise unchanged, an entire region of the parent scaffold backbone is replaced with
201 the backbone of the secondary structure containing the desired epitope. This allows the grafting
202 of more complex epitopes that have no existing structural match, such as the CC40.8 S2-helix
203 epitope. Candidate scaffolds were identified by aligning the N- and C-termini of the stem helix
204 epitope in its CC40.8-bound conformation with the N- and C-termini of possible insertion sites on
205 candidate scaffolds (**Figure 3a, b**). For scaffolds where the backbone RMSD of this alignment
206 was below 0.75Å, the epitope replaced the overlapping backbone of the parent scaffold, and
207 additional mutations were introduced to integrate the epitope into the scaffold and to ensure
208 productive interactions with CC40.8 mAb (**Figure 3a**). The structures of candidate designs were
209 predicted using Alphafold2[21], and additional mutations were introduced to ensure proper epitope
210 conformation. Final designs contained between 16 to 32 mutations relative to the parent scaffolds,
211 and the grafted epitope was 3.1 to 6.7Å away by RMSD from the backbone it replaced.

212 Six epitope scaffolds, named S2hlx-Ex1 to 6 (**Figure 3b** for representative models; **Supp.**
213 **Table 1**) were tested for bacterial expression and analyzed for binding to S2P6 mAb in an initial
214 screen. While four of the six designs, S2hlx-Ex2, -Ex3, -Ex4 and -Ex6, bound to S2P6, three of

215 them those had poor expression (S2hlx-Ex2, -Ex4 and -Ex6) (**Supp. Fig. 10**). To improve
216 expression, we tested different protein expression tags and evaluated structural homologs of the
217 parent scaffolds as alternative design templates with limited success (**Supp. Figs. 11, 12**). Next,
218 we optimized the sequence of the S2hlx-Ex designs using ProteinMPNN[22], a recently described
219 deep learning algorithm that takes a protein structure as input and generates amino acid
220 sequences that are predicted to generate the same fold. All four backbone grafting designs that
221 bound S2P6, S2hlx-Ex2, -Ex3, Ex4, and -Ex6, were optimized with this approach, and sequences
222 that expressed with high yield (40mg/L of culture on average, **Supp. Fig. 13**) were identified for
223 all of them. For a given structure, ProteinMPNN generated designs that had highly different
224 sequences outside the epitope (**Figure 3b**). For example, S2hlx-Ex2 based designs -Ex15, -Ex17,
225 -Ex19, -Ex20 had between 42% and 55% amino acid sequence identity with the S2hlx-Ex2
226 template (**Figure 3c**), and only 58-75% identity with each other, yet all bound to the stem helix
227 mAbs by ELISA (**Supp. Figure 14**).

228 The binding affinities for the various ProteinMPNN designs based on the backbones of
229 S2hlx-Ex2 (*S2hlx-Ex15, -Ex17, -Ex19, and -Ex20*), S2hlx-Ex3 (*S2hlx-Ex46 and S2hlx-Ex54*),
230 S2hlx-Ex4 (*S2hlx-Ex8-Trx and S2hlx-Ex25*), and S2hlx-Ex6 (*S2hlx-Ex34 and -Ex37*) to CC40.8,
231 S2P6, and DH1057.1 mAbs were determined by SPR (**Supp. Fig. 15, 16)**. S2hlx-Ex2 derived
232 epitope scaffolds had the highest affinities with dissociation constants between 2nM and 30nM
233 for S2P6, 2nM and 49nM for DH1057.1, and 3nM to 27nM for CC40.8 mAb (**Figure 3d; Supp.**
234 **Fig. 15**). S2hlx-Ex15 and -Ex19 had affinities in a similar range to those measured for spike (**Supp**
235 **Fig. 8)** and those reported for the stem helix peptide[9,10]. S2hlx-Ex54, derived from the backbone
236 of S2hlx-Ex3, bound to S2P6, DH1057.1, and CC40.8 with equilibrium dissociation constants of
237 45nM, 222nM and 150nM respectively (**Supp. Fig. 16**), while S2hlx-Ex37, based on the fold of
238 S2hlx-Ex6, had affinities of 664nM, 220nM and 849nM to the three target mAbs (**Supp. Fig. 16**).

239 To test the ability of epitope scaffolds to engage diverse antibodies that may be elicited
240 as part of a polyclonal response against the stem helix by vaccination, the designed antigens
241 were tested against additional broadly reactive stem helix antibodies that were recently described
242 and were not explicitly targeted at the design stage[23]. The epitope scaffolds bound all tested
243 antibodies by ELISA (**Figure 3e; Supp. Fig. 17a)**, indicative of their ability to recognize diverse
244 antibodies that target the displayed epitope. In addition to the mature antibodies, binding was also
245 tested to five of their UCA or inferred germline precursors (**Figure 3e; Supp. Fig. 17b**). Kinetic
246 analysis revealed that S2hlx-Ex15 had low nanomolar affinities for DH1057 UCA and the iGLs for
247 S2P6 and CC40.8 (K_Ds of 22.4nM 1.4nM and 9.7nM), and also bound strongly to Cov44-26 UCA
248 and Cov89-22iGL by ELISA. Other S2hlx-Ex2 and S2hlx-Ex3 derived designs interacted similarly
249 with three to five of the antibody precursors tested (**Figure 3d, Supp. Fig. 15**). Four out of the
250 five antibody precursor recognized spike, but with significantly weaker affinity than S2hlx-Ex15
251 and S2hlx-Ex19 (**Supp. Fig. 17**).

252 To ensure that the S2hlx epitope scaffolds interacted with the target mAbs in a similar
253 fashion to spike, antibody binding was measured to eight epitope scaffolds that spanned all the
254 design families (**Figure 3b**) and that contained alanine mutations corresponding to spike epitope
255 sites Leu1145 and Phe1148 in the stem helix (**Supp. Fig. 18**). As anticipated based on structural
256 analysis and previously published observations[10], all the epitope scaffolds lost binding to CC40.8
257 when the Leu1145 equivalent residue was mutated, while binding to S2P6 and DH1057.1 was
258 not affected. When the epitope residue equivalent to spike Phe1148 was mutated, binding was
259 lost to DH1057.1 and S2P6 in all designs, confirming that antibody interactions are mediated by
260 the same residues on spike and the designed antigens.

261 Analysis of a high-resolution (2.3Å) crystal structure of unbound S2hlx-Ex19 further
262 confirmed the successful transplantation of the CC40.8 mAb epitope (**Figure 3f, Supplemental**
263 **Table 2**). As expected, the grafted epitope region in S2hlx-Ex19 diverged considerably from the

264 backbone region it replaced in the parent scaffold (backbone RMSD=5.8Å), with the epitope
265 adopting a more exposed conformation that allows for antibody engagement (**Figure 3f**). This
266 conformational change was likely facilitated by introducing two aromatic residues (Tyr62 and
267 Phe66) under the epitope helix, which effectively pushed the epitope segment away from the rest
268 of the protein core. Interestingly, the epitope conformation on S2hlx-Ex19 was almost identical to
269 that present on the prefusion stem helix, rather than the more extended one induced by CC40.8
270 (**Figure 3f**). Nevertheless, given the high affinity of S2hlx-Ex19 for CC40.8 (K_D=6.7nM), it is likely
271 that the antibody can readily induce the necessary conformation upon binding. Thus, by
272 combining epitope backbone grafting and ProteinMPNN, we engineered antigens that bind with
273 high affinity and specificity to the major classes of stem helix broadly reactive antibodies as well
274 as to their inferred precursors.

275 **Cross-reactivity of engineered epitope scaffolds with pre-existing immune**
276 **responses induced by SARS-CoV-2 spike.**

277 Next, we tested the ability of the engineered epitope scaffolds to cross-react with pre-
278 existing immune responses elicited by SARS-CoV-2 spike in order to evaluate their potential to
279 preferentially amplify spike$^{815-823}$ or stem helix directed responses by vaccination. Sera or plasma
280 samples isolated from three groups of 12 study participants who acquired SARS-CoV-2 immunity
281 either through vaccination, infection, or vaccination followed by infection respectively, were first
282 tested for binding to WA-2 spike, RBD and synthesized peptides encoding the spike$^{815-823}$ and
283 stem helix regions (see **Supp. Table 3** for full patient information). This analysis revealed that
284 only a small fraction of spike-directed humoral responses, regardless of their acquisition route,
285 targeted the spike$^{815-823}$ or stem helix regions (**Figure 4a**). On average, spike$^{815-823}$ and stem helix
286 peptide binding levels were 23.3 and 8.4-fold lower respectively than RBD-focused responses
287 across all groups, underscoring that the spike$^{815-823}$ and the stem helix domains are sub-dominant
288 targets of antibodies elicited by spike.

289 Both spike$^{815-823}$ and S2hlx-Ex epitope scaffolds showed significantly higher recognition of
290 human sera than the corresponding spike peptide domains (**Figure 4a, Supp. Fig. 19)**. Among
291 the spike$^{815-823}$ epitope scaffolds, FP-15 had the best sera recognition, showing 11.3, 7.7, and 5.8-
292 fold higher IgG binding than the corresponding synthesized peptide in vaccinated, infected and
293 hybrid immunity samples respectively (**Figure 4b)**. Importantly, these interactions were mediated
294 by the engineered epitope contacts, as binding to the parent scaffold of FP-15 that does not
295 contain the grafted epitope, was significantly reduced (3.5 -fold in vaccinated, 2.5-fold in infected
296 and 5.5-fold in hybrid, **Figure 4b**). A similar trend was observed for FP-10 and FP-2, but their
297 overall binding levels were lower than FP-15, although still above those of the synthesized
298 spike$^{815-823}$ peptide (**Supp. Fig. 19b)**.

299 From the stem helix designs, S2hlx-Ex19 and S2hlx-Ex15 had the best recognition of
300 spike-induced immune responses **(Supp. Fig 19a)**. Compared to the synthesized stem helix
301 peptide, S2hlx-Ex19 bound on average 2.4 times better across all three groups (**Figure 4c)**. The
302 binding was epitope specific, as evidenced by the decrease in interactions with S2hlx-Ex19
303 variants that contained alanine mutations at hotspot epitope residues Leu1145 (LA) and Phe1148
304 (FA), or that had the whole epitope replaced by the sequence of the parent scaffold (S2hlx-Ex19
305 PShlx, **Figure 4c**). As shown by the larger decrease in binding to the FA than LA mutants, cross-
306 reactive spike responses were more dependent on stem helix residue Phe1148 which is
307 recognized by both S2P6 and CC40.8 classes of antibodies (**Figure 4c, Supp. Fig 19**). Compared
308 to S2hlx designs, the ability of the S2hlx-Ex epitope scaffolds to recognize CC40.8 mAb translated
309 into a broader engagement of spike elicited humoral responses for these types of molecules
310 (**Figure 4a, Supp. Fig 19**).

311 **Isolation of antibodies with broad coronavirus reactivity from humans pre-exposed**
312 **to SARS-CoV-2 using epitope scaffolds.**

313 Next, we characterized the ability of the engineered epitope scaffolds to interact with B
314 cells that give rise to antibodies with broad activity against the spike$^{815-823}$ peptide or the stem
315 helix from people with preexisting SARS-CoV-2 immunity, as a way to evaluate the potential of
316 our immunogens to boost such responses by vaccination. Stem helix reactive BCRs were isolated
317 from IgD- B cells, a pool that included both memory B cells and plasmablasts, from the two
318 subjects with the highest sera titers against S2hlx-Ex19, using positive selection for S2hlx-Ex19
319 and negative selection for the parent scaffold S2hlx-Ex19-PS that lacks the epitope (**Figure 5a,b**).
320 Stem helix epitope-specific memory B cells were isolated at a frequency of ~1:3000 and ~1:2100
321 respectively from the two samples (**Figure 5b, Supp. Fig 20)**.

322 Antibody sequences were amplified from the isolated B cells and preliminarily screened
323 for spike binding[24] in order to select monoclonal antibodies for recombinant production and in-
324 depth functional characterization. Twelve recombinant antibodies selected from B cells that bound
325 S2hlx-Ex19 but not S2hlx-Ex19-PS were tested for binding against a panel of spike proteins from
326 SARS-CoV-2 variants as well as other human and animal betacoronaviruses. Ten antibodies
327 showed measurable affinity to multiple coronavirus spikes, with three of them displaying binding
328 on par to that of S2P6 and CC40.8 mAbs to all the spikes tested, including SARS-CoV-1, MERS,
329 OC43 and HKU-1 (**Figure 5c, Supp. Figs. 21-24**). Interestingly, these three antibodies,
330 DH1501.1, DH1501.2, and DH1501.3, were clonally related and their heavy and light chain V
331 gene segment pairing (IGHV1-46/IGKV3-20) matched those of S2P6 mAb. The inferred UCA of
332 these antibodies displayed tight binding to multiple spikes, similar to what was reported for the
333 iGL of S2P6 mAb (**Supp. Fig. 25**). Beyond the IGHV1-46/IGKV3-20 derived mAbs, multiple other
334 unique V_H/V_L pairings, not previously reported, were observed in the isolated antibodies (**Figure
335 5c**). This suggests the presence of a clonally diverse response against the stem helix epitope that
336 can be engaged by the engineered epitope scaffold. The best six antibodies by affinity and
337 breadth were tested side by side with S2P6 and CC40.8 for their ability to neutralize multiple

338 SARS-CoV-2 variants and SARS-CoV-1 in a pseudovirus neutralization assay. CC40.8 and two
339 isolated mAbs, DH1501.1 and DH1501.3, were the only ones that displayed neutralization activity,
340 albeit with high IC_{50} values above 1μg/mL that are typical for antibodies against this epitope.
341 DH1501.3 and CC40.8 neutralized all the pseudoviruses in the panel, including XBB1.5 and
342 SARS-CoV-1 (**Figure 5d**).

343 Given that stem helix antibodies were previously shown to protect against infection in
344 animal models despite limited neutralization potency[9,10], we next investigated whether the isolated
345 monoclonal antibodies could control the virus through antibody-mediated functions. To determine
346 the ability of these mAbs to mediate Fc effector functions, they were first tested for binding to
347 virus-infected cells, a prerequisite of antibody-dependent cellular cytotoxicity (ADCC). Three of
348 the five antibodies tested, DH1501.1, DH1501.2, and DH1501.3, showed binding to cells infected
349 with either the D614G or the BA.1 variant of SARS-CoV-2 in the same range as the previously
350 described stem helix antibodies CC40.8, S2P6 and DH1057.1 (**Figure 5e**). Binding of the stem
351 helix antibodies was lower that of the RBD-directed mAb DH1047, supporting the observation that
352 the stem helix epitope is more occluded on the viral spike. Next, we performed a Natural Killer
353 (NK) cell degranulation assay as a surrogate for assessing ADCC activity. Antibodies DH1489,
354 DH1501.1, DH1501.2, and DH1501.3 induced NK cell degranulation against all three variants of
355 concern tested, with potencies similar to those of known stem helix antibodies (**Figure 5f**).
356 Interestingly, all stem helix mAbs induced the most potent degranulation against BA.4/5 spike-
357 transfected cells. Overall, isolated antibodies with IGHV1-46/IGKV3-20 immunogenetics had the
358 highest activity in both the pseudovirus neutralization and ADCC assays. While other isolated
359 antibodies with different V_H/V_L pairings were not as broad or potent, it is possible that they could
360 be further matured to breadth by targeted vaccination and may be valuable targets for rational
361 vaccine design.

362 We similarly isolated antibodies against the spike$^{815-823}$ epitope by sorting B cells that
363 bound the FP-10 epitope scaffolds and lacked binding to the original parent scaffold that did not
364 contain the grafted epitope. The frequency of epitope specific B cells selected was ~1:4,000 in
365 two analyzed samples and two antibody sequences were recovered for recombinant expression
366 and characterizations after preliminary screening. These antibodies had distinct immunogenetics
367 not observed in other previously isolated antibodies against the spike$^{815-823}$ epitope (**Figure 5c**).
368 Nevertheless, they bound tightly to diverse coronavirus spikes, including those of human alpha
369 coronaviruses 229E and NL63 as is typical of antibodies with broad activity against this epitope
370 (**Figure 5c**). No binding was detected for SARS-CoV-2 variants BA.1 and XBB1.5, however these
371 recombinant spikes contained a "hexapro" mutation that is known to affect the presentation of the
372 spike$^{815-823}$ epitope and to limit the binding of antibodies against this site[8].

373 Antibody isolation from subjects with pre-existing SARS-CoV-2 immunity revealed that the
374 engineered epitope scaffolds interact with diverse monoclonals against the target epitopes. Some
375 of the antibodies are derived from the same V_H and V_L genes observed in antibodies previously
376 isolated[9]. While the epitope scaffold reactive mAbs against the stem helix had weak neutralization
377 potency, they exhibited strong ADCC activity *in vitro*, revealing a potential protection mechanism
378 consistent with previous observations for this antibody class. Taken together, the robust sera
379 binding and memory B cell engagement by epitope scaffolds demonstrate their strong recognition
380 of pre-existing SARS-CoV-2 immune response and support their use for boosting spike$^{815-823}$ and
381 stem helix antibodies by vaccination.

382 **Engineered stem helix epitope scaffolds elicit antibodies with broad reactivity**
383 **against diverse CoVs by vaccination.**

384 Next, we assessed the ability of the engineered epitope scaffolds to elicit antibodies
385 against the target epitope by vaccination. We focused on testing the stem helix immunogens

386 belonging to the S2hlx-Ex2 family of design, Ex15, Ex19, Ex20, and Ex17, because: 1) they have
387 high affinities for all the antibodies tested as well as their precursors; and 2) while they share the
388 same backbone structure, their sequence outside the epitope is highly divergent, which may help
389 focus immune responses on the epitope by vaccinating with combinations of different designs.

390 Epitope scaffolds were multimerized on mi03 nanoparticles (NPs) using the
391 SpyCatcher/Spytag[25] conjugation system in order to improve immune presentation **(Figure 6a)**.
392 Homotypic nanoparticles were developed that displayed 60 copies of designs Ex15, Ex19, or
393 Ex20 respectively. A "mosaic" NP was also engineered where Ex15, Ex19, Ex20, and Ex17 were
394 conjugated together. Antigenic and NSEM characterization confirmed that the NPs were well
395 formed and bound S2P6, DH1057.1 and CC40.8 (**Supp. Fig. 26**). Groups of eight BALB/c mice
396 were vaccinated three times, four weeks apart with either: 1) Ex15-NP; 2) Ex_mosaic-NP; 3) a
397 mixture of individual Ex15-NP, Ex19-NP and Ex20-NP; 4) a sequential regimen of Ex15-NP prime,
398 followed by Ex19-NP and Ex20-NP boosts; or 5) GLA-SE only, the adjuvant included in all the
399 immunizations, as control **(Figure 6b)**. After two immunizations, sera from all animals vaccinated
400 with epitope scaffolds showed strong reactivity to WA-2 and XBB SARS-CoV-2 spikes **(Figure**
401 **6c)**. Sera breadth was tested against spikes from all human beta coronaviruses as well as
402 RsSHC014 and GXP4L, two pre-emergent animal viruses from bats and pangolins. Binding was
403 observed against all the spikes tested, with the highest activity against SARS-CoV-1, RsSHC014,
404 and GXP4L **(Figure 6d)**. Importantly, sera cross-reacted with OC43, MERS, and HKU-1 spikes,
405 although at lower levels than those measured against SARS-CoV-2, but consistent with the
406 induction of a broad response against the stem helix epitope **(Figure 6d)**. Of the four immunization
407 regimens tested, the homotypic Ex15 NP elicited the lowest titers and breadth. Combinations of
408 epitope scaffolds whether administered together, in mosaic form or sequentially, performed
409 similarly well, although the Ex_mosaic-NP elicited the highest average titers against heterologous
410 human betacoronaviruses.

411 Epitope specificity was demonstrated by strong sera binding to an unrelated epitope
412 scaffold not used in the immunizations **(Supp. Fig. 27)**. Epitope specificity was further
413 demonstrated by measuring binding to synthesized peptides encoding the stem helix region as
414 well as mutated variants at sites known to be important for antibody recognition (**Figure 6e**).
415 Mutations at residues 1148, 1152, and 1156 decreased sera binding, while alanine substitution
416 at position 1145 had limited effect, consistent with the elicitation of antibodies that resemble the
417 binding mode of S2P6 or DH1057.1, rather than that of CC40.8 (**Figure 6e**). No neutralizing
418 activity was observed for the elicited sera, which was unsurprising given the limited activity of
419 S2P6-like recombinant monoclonals in our pseudovirus neutralization assay **(Figure 5d)**.

420 Next, we assessed the ability of the Ex_mosaic-NP to boost stem helix specific responses
421 in animals previously vaccinated with mRNA encoding the SARS-CoV-2 WA-2 spike and to
422 protect against a viral challenge with a heterologous virus. Assessing protection was particularly
423 important since sera elicited by stem helix epitope scaffolds did not neutralize in our assay;
424 however, antibodies that react with the grafted epitope can promote strong ADCC as shown
425 above (**Figure 5e,f**) and may protect through antibody-mediated functions. K18-ACE2 mice were
426 immunized every four weeks with either four shots of mRNA spike or twice with mRNA spike
427 followed by two boosts of the Ex_mosaic-NP. Two weeks after the last immunization, the animals
428 were challenged with live WIV-1 virus (**Figure 6f**). WIV-1 was chosen because its spike sequence
429 is significantly different from that of SARS-CoV-2 (78% over the whole spike and 75% over RBD),
430 while the stem helix epitope sequence is conserved, as in most sarbecoviruses. Animals
431 vaccinated with Ex_mosaic-NP had higher average titers of antibodies targeting the stem helix
432 epitope compared to those that received only spike mRNA, as measured by binding to an epitope
433 scaffold not used in the immunization; binding to the synthesized stem helix peptide was also
434 higher, but not statistically significant (**Supp. Fig. 28**). Both immunizations regimens provided
435 strong protection from WIV-1 based on the percentage of body weight the animals lost six days

436 after the challenge and when compared to animals that received adjuvant only (**Figure 6g**).
437 However, animals boosted with Ex_mosaic-NP scored better on two other clinical measures
438 compared to those that received spike mRNA only. No viral RNA was detected in the lungs of any
439 of the Ex_mosaic-NP immunized animals and their congestion scores were significantly lower
440 when compared to those of mRNA spike vaccinated animals (**Figure 6h**). These results
441 demonstrate that stem helix epitopes elicit sera with broad reactivity against beta coronaviruses
442 and can offer protection against divergent viruses when used to boost immune responses initially
443 induced by mRNA spike immunizations.

444 Discussion

445 While currently approved coronavirus vaccines and multiple vaccine candidates are based
446 on spike or RBD proteins[26], here we describe new types of immunogens that aim to elicit different
447 humoral responses, focused on the conserved stem helix or the spike$^{815-823}$ epitopes in the S2
448 domain of spike. The ability to elicit high titers of antibodies against these regions will likely be
449 critical to the development of a pan-coronavirus vaccine[27], a goal the molecules designed here
450 aim to contribute towards. The epitope scaffold proteins were engineered using a combination of
451 previously developed grafting methods[15,28] and more recently described machine learning
452 techniques[29] that proved critical for improving both immunogen stability and antigenicity.
453 Structural and mutational analysis confirmed that the epitope scaffolds engage multiple
454 antibodies, as well as their precursors, with high affinity and specificity. For each class of epitope
455 scaffolds, some designs showed tighter antibody binding than corresponding epitope peptides,
456 especially as it relates to the recognition of antibody precursors.

457 Spike$^{815-823}$ and stem helix epitope scaffolds that bound S2P6 and DH1058 mAbs, but not
458 CC40.8 mAb, were engineered using side chain grafting, an approach that modifies the sequence
459 of existing proteins to accommodate the epitope and that was successfully used in the past to

460 engineer epitope scaffolds against HIV[18,30,31] and RSV[32] antibodies. However, for conformationally
461 complex epitopes like the one induced by the CC40.8 mAb on spike, no known protein structures
462 may exist that are structurally similar to allow side chain grafting. To successfully transplant these
463 types of epitopes, different methods, called flexible backbone approaches, are needed to model
464 and control the conformation of the epitope on the target scaffolds. This can be achieved either
465 by engineering epitope scaffolds *de novo* by folding idealized protein backbones around the target
466 epitope, as was previously done for epitopes on RSV[19,33], or by modifying the backbone of existing
467 proteins to adopt the conformation of the grafted epitope, as illustrated before for HIV[28,30] and
468 here for designs that bind CC40.8 mAb. Previously, the success of flexible backbone epitope
469 grafting was limited; the majority of the computational designs failed to express recombinantly
470 and the ones that did typically required multiple rounds of directed evolution to achieve high
471 affinities to the target antibodies.

472 Here we combined previously described backbone grafting with recent machine learning
473 based protein engineering approaches to significantly improve the success rate of epitope
474 scaffolds designed using flexible backbone modeling. Structure prediction with AlphaFold2[34] was
475 used to validate the conformation of the grafted epitope in the structural context of the target
476 scaffold, while ProteinMPNN[22] was subsequently employed to identify optimal sequences that
477 fold into the desired epitope scaffold structure. With this approach, multiple proteins were
478 engineered *in silico* that bound tightly to CC40.8 mAb without needing additional experimental
479 optimization. Of note, the epitope was successfully transplanted on scaffolds with diverse
480 backbone structures, supporting our approach as a general way to present structurally complex
481 motifs in diverse molecular contexts. Development of stem helix epitope scaffolds that bound with
482 high affinity to all three target antibodies (S2P6, DH1057.1, CC40.8) proved challenging because
483 CC40.8 induces a different conformation on the epitope upon binding compared to the other two
484 antibodies. This suggests that, for a successful design, the epitope presentation must allow for

485 antibody-induced fit and some level of conformational changes. This was not explicitly modeled
486 here at the design stage but likely represents an area of improvement in the computational
487 workflow for transplanting epitopes that adopt different antibody-bound conformations in the
488 future. Interestingly, the stem helix immunogen S2hlx-Ex19, which bound with affinities for
489 CC40.8 and S2P6 similar to those of the native spike, displays the epitope at the N-terminus of
490 the scaffold. While a crystal structure of this unbound epitope scaffold revealed that the epitope
491 is well folded and adopts a helical conformation, it is possible that its positioning may more readily
492 allow for conformational changes upon antibody binding relative to other designs where the
493 epitope is grafted internally.

494 The ability of engineered immunogens to engage diverse antibodies against the displayed
495 epitope is likely important for their ability to elicit a robust polyclonal response *in vivo*, as has been
496 recently demonstrated for HIV vaccine candidates[35,36]. The epitope scaffolds designed here
497 engaged multiple spike[815-823] and stem helix antibodies with high affinity *in vitro*, which translated
498 to robust reactivity to polyclonal sera elicited by SARS-CoV-2 and the engagement of BCRs with
499 diverse immunogenetics against the target epitopes. The stem helix epitope scaffolds that also
500 bound CC40.8 mAb in addition to S2P6 and DH1057.1 mAbs, showed the highest level of binding
501 to human sera from subjects exposed to SARS-CoV-2 by vaccination, infection or both. The
502 S2hlx-Ex19 design was used to isolate multiple antibodies with broad reactivity against the stem
503 helix from people with pre-existing immunity. Some of these monoclonal antibodies had the same
504 V_H/V_L pairings (IGHV1-46/IGKV3-20) as previously isolated antibodies, suggesting that this type
505 of antibody is commonly induced by SARS-CoV-2 immunization and may be targeted for boosting
506 with a next-generation vaccine. However, as found here, other broad antibodies with different
507 immunogenetic characteristics exist against S2 and they can be engaged by the designed epitope
508 scaffolds as well. Isolated stem helix antibodies displayed limited neutralization against SARS-
509 CoV-2 variants, consistent with previous reports describing other antibodies against this

510 epitope[9,37]. Interestingly, despite their limited neutralization, stem helix antibodies were shown by
511 others to protect well against live virus challenges[9,37], likely through their antibody-mediated
512 functions which we demonstrated our antibodies also have.

513 In initial immunization studies, stem helix epitope scaffolds elicited sera with broad
514 reactivity against all human beta coronaviruses and towards two animal viruses tested. Sera
515 bound specifically to the target epitope in a manner consistent with the induction of S2P6-like
516 mAbs. Future studies will analyze the B cell repertoire of vaccinated animals in more detail to
517 better understand the specificity and protection ability of the elicited responses. The induced sera
518 did not neutralize SARS-CoV-2 pseudoviruses in our assay, consistent with our observations and
519 previous reports that antibodies against the stem helix are poor neutralizers, but can protect
520 through antibody mediated functions[9,37]. To demonstrate that the engineered immunogens can
521 protect against coronavirus infection, we vaccinated K18-ACE mice pre-exposed to spike mRNA
522 with stem helix immunogens, prior to a viral challenge with WIV-1. Compared to an adjuvant-only
523 group, mice boosted with our immunogens were protected against weight loss, had limited lung
524 congestion, and undetectable viral load in the lungs. While mice immunized with only mRNA spike
525 were also protected against weight loss, they exhibited increased congestion and higher titers of
526 lungs viremia compared to mice that received the stem helix epitope scaffolds. Taken together,
527 these results support the continued development and characterization of epitope scaffold
528 immunogens to boost responses against conserved S2 epitopes as part of a next-generation pan
529 betacoronavirus vaccine.

530

531

532

533 **Acknowledgments**

534 We thank Whitney Edwards Beck, Deborah Murray, Micah McClain, Thomas Burke, Jack
535 Anderson, Lynn Harrington, Christopher Todd and Kathlene Chmielewski for help with acquiring
536 and managing the human samples. We thank Aria Arus-Altuz for developing the fluorescent
537 probes used for FACS. We thank Brian Watts, Ken Cronin and Alam Munir for their assistance at
538 the DHVI Biomolecular Interaction Analysis (BIA) Core Facility. We thank Wes Rountree and
539 Yunfei Wang for the statistical analysis. We thank Advaita Sing and Christopher O'Donnell from
540 the Azoitei lab for their help. We thank Jacob Gater and Pahvie Chhan from the Duke Human
541 Vaccine Institute Small Animal Team for their help with the immunization studies. We thank
542 Priyamvada Acharya and Jared Lindenberger for their help with crystallization experiments.
543 Structural results shown in this report are derived from data collected at Southeast Regional
544 Collaborative Access Team (SER-CAT; 22 ID and 19 BM) beamlines at the Advanced Photon
545 Source, Argonne National Laboratory. Use of the Advanced Photon Source was supported by the
546 U. S. Department of Energy, Office of Science, Office of Basic Energy Sciences, under Contract
547 No. W-31-109-Eng-38.

548 **Funding**: This work was supported by grants P01AI158571 (B.F.H) and R01AI155804
549 (M.L.A) from the National Institute of Allergy and Infectious Diseases of the National Institute of
550 Health and by a Duke School of Medicine COVID Award (M.L.A).

551 **Author Contribution.** MLA, BK, and DJM: conceptualization, methodology, study design,
552 and immunogen engineering; BK, CH, CB, KW, DJM, and BR performed *in vitro* characterization
553 of epitope scaffold immunogens; BK, DW, and KW performed the crystallographic analysis; QY,
554 LX, AF, RP, MB, KOS, and DWC performed the B cell isolation, sequencing and antibody
555 identification; AE and DM performed the pseudovirus neutralization assay; DM, BM, TK, SSO, GF
556 performed NK degranulation analysis; AN, CH, AS, JMF, AH, NJC performed the animal

immunization, the viral challenge experiments and their analysis; CW, EQP, EBW, KW, KOS, RB, and BFH: resources; KW and EVI preformed unmutated common ancestor interference; KM and RJE performed NSEM analysis; figure development; MLA, DJM, BK: writing, original draft; MLA, DJM, BK, BFH, DW, KW, KOS, DM, GF, AE, DM, AN, AS, XL, EVI: writing, review and editing; MLA, BFH, KW, KOS: funding acquisition; MLA: project administration and supervision.

Competing interests: MLA, BFH, DJM and BK submitted a patent application that covers the engineered epitope scaffolds. The other authors declare no competing interests.

Data and materials availability: Crystal structures have been deposited in the PDB under accession numbers 8F5I, 8FDO and 8F5H. The epitope scaffold can be obtained through an MTA from the corresponding author. Other reagents are available upon requests.

572 # Materials and methods

573 **Computational design of epitope scaffolds.**

574 *Design of epitope scaffolds by side chain grafting.* A database of 9884 candidate scaffolds was
575 created by selecting from the Protein Data Bank (PDB) structures that were: 1) determined by x-
576 ray crystallography; 2) high resolution (<2.8 Å); 3) monomeric; 4) expressed in *E. Coli*; 5) not of
577 human origin and 6) that did not contain ligands. Epitope scaffolds were designed with Rosetta
578 as previously reported, using the RosettaScripts for side chain grafting described in *Silva et. al*.,
579 with the following parameters in the *MotifGraft* mover: RMSD_tolerance="0.3";
580 NC_points_RMSD_tolerance="0.5"; clash_test_residue="ALA"; clash_score_cutoff="5". For the
581 design of spike$^{815\text{-}823}$ peptide (FP) epitope scaffolds, the structure of spike$^{815\text{-}823}$ peptide fragment
582 ^{815}RSFIEDLLF^{823} as described in the crystal structure of the DH1058-FP peptide complex (PDBid:
583 7tow) was used as the target epitope to graft. With the exception of residues F817 and L821 which
584 were allowed to change in the designed epitope scaffold because they did not contribute to
585 antibody binding, the identity of all the other epitope residues was maintained. For the design of
586 epitope scaffolds that bind S2P6 and DH1057.1 mAbs, the structure of the stem helix fragment
587 ^{1148}FKEELDKYF$^{1156\ \text{from}}$ PDBid:7rnj was grafted. The identity of residues E1150 and K1154 was
588 allowed to change during the design process while the other epitope residues were kept fixed.
589 From the epitope scaffold generated by the automated protocol, the top 100 models by Rosetta
590 ddG that were also smaller than 150 amino acids were visually examined to ensure appropriate
591 epitope transplantation and antibody-scaffold interaction. At this stage, the suitability of a given
592 parent scaffold in terms of function, conformational flexibility, and expression protocol was also
593 investigated by referencing the publication it originated from. If necessary, additional changes
594 were introduced in a candidate epitope scaffold using Rosetta fixed backbone design to remove
595 antibody-epitope scaffold contacts that were not due to the target epitope and to ensure proper

interactions between the epitope and the rest of the scaffold. The best 15 designs for each of the target epitopes were chosen for experimental characterization.

Design of stem helix epitope scaffolds by backbone grafting and MPNN optimization.

Epitope scaffolds that display the stem helix epitope recognized by the CC40.8 antibody (PDBid: 7sjs) were designed by backbone grafting as previously reported and using the RosettaScripts described by Silva et. al. The same set of curated parent scaffolds as the one used for side chain grafting above was searched here. The structure of the stem helix fragment ^{1144}ELDSFKEELDKYFK^{1157} from PDBid:7sjs was grafted. The identity of residues E1144, D1146, S1147, E1150, K1154, and K1157 were allowed to change during the design process while the other epitope residues were kept fixed. The following parameters were used:

```
RMSD_tolerance="5.0" NC_points_RMSD_tolerance="0.75"
clash_score_cutoff="5" clash_test_residue="ALA"
hotspots="2:5:6:8:9:10:12:13"
combinatory_fragment_size_delta="1:1”
max_fragment_replacement_size_delta="-4:4"
full_motif_bb_alignment="0"
allow_independent_alignment_per_fragment="0"
graft_only_hotspots_by_replacement="0"
only_allow_if_N_point_match_aa_identity="0"
only_allow_if_C_point_match_aa_identity="0"
revert_graft_to_native_sequence="0"
allow_repeat_same_graft_output="0" />
```

The initial hits were filtered to remove scaffolds with (1) an average clash score greater than 5 across the epitope, and (2) a Rosetta calculated ddg greater than 0. The top 100 models by Rosetta ddG that were also smaller than 150 amino acids were then visually examined as

621 above and then Alphafold2 was used to predict the structure of the 10 best designs using the
622 following parameters-

623 --model_preset=monomer
624 --db_preset=full_dbs
625 --max_template_date=2021-11-01
626 --uniref90_database_path=/data/uniref90/uniref90.fasta
627 --mgnify_database_path=/data/mgnify/mgy_clusters.fa
628 --uniclust30_database_path=/data/uniclust30/uniclust30_2018_08/uniclust30_2018_08
629 --bfd_database_path=/data/bfd/bfd_metaclust_clu_complete_id30_c90_final_seq.sorted_opt
630 --template_mmcif_dir=/data/pdb_mmcif/mmcif_files
631 --obsolete_pdbs_path=/data/pdb_mmcif/obsolete.dat
632 --pdb70_database_path=/data/pdb70/pdb70

633 The scaffolds were then aligned via the grafted epitope to the stem helix fragment in the
634 CC40.8 structure PDBid:7sjs and inspected for clashes between the scaffold and antibody.
635 Scaffolds with clashes, such as where the antibody binding epitope was occluded or buried, were
636 modified such that key epitope residues above remained fixed while other residues in the epitope
637 and in contacting parts of the scaffold were allowed to vary through iterative rounds of fixed-
638 backbone rotamer-based sequence design in Rosetta. After each round, we checked the
639 Alphafold2 prediction and repeated until the epitope was predicted to be presented in a suitable
640 orientation for antibody binding (**Figure 3a**). Expression tags were screened by N-terminally
641 tagging S2hlx-Ex4 with GST, SUMO, Thioredoxin (Trx), Maltose binding protein (MBP), or F8H
642 tags. As Trx gave the highest fraction of full-length protein it was then used to tag S2hlx-Ex2 and
643 -Ex6 (**Supp. Fig. 11**).

644 The parent structure of S2hlx-Ex4 (PDBid:2QYW) was used to screen the VAST+
645 database (https://structure.ncbi.nlm.nih.gov/Structure/VAST/vast.shtml) for homologous

646 structures, which were identified by RMSD (<2Å) and high fraction of alignment (>80%). Two
647 homologs identified were expressed with Trx tags (**Supp. Fig. 12**).

648 For ESs where protein expression was low the protein structures, either the Rosetta model
649 or Alphafold prediction, were entered into ProteinMPNN at the website,
650 https://huggingface.co/spaces/simonduerr/ProteinMPNN. Initial designs for S2hlx-Ex2 and -4
651 used sampling temperature of 0.1 and backbone noise of 0.02 and the whole epitope sequence
652 was fixed, For S2hlx-Ex2, this approach produced six related soluble ESs but failed for S2hlx-
653 Ex4. The second set of S2hlx-Ex4 and S2hlx-Ex6 designs used the higher sampling temperature
654 (0.25) and higher backbone noise (0.2) to increase sequence diversity in designs, and only
655 L^{1145}xxFKxELDxYF^{1156} residues were fixed. ES structures were modelled using the integrated
656 Colabfold prediction and scored by RMSD and pLDDT, and the highest scoring were re-predicted
657 using Alphafold2. For the S2hlx-Ex6 designs, the epitope was occluded or buried in several
658 designs. In these cases, residues in the epitope or surrounding parts of the ES were manually
659 modified and the ES structure prediction repeated using Alphafold2 until the epitope was
660 predicted to be suitable to binding to S2P6.

661 **Plasmids and DNA synthesis.**

662 Genes encoding designed epitope scaffolds were commercially synthesized and cloned
663 into pET29b (Genscript). Genes encoding the antibody heavy and light chains were similarly
664 synthesized and cloned into the pcDNA3.1 vector (GenScript). Oligonucleotides were synthesized
665 by IDT. Mutations were introduced in the synthesized plasmids by Q5 mutagenesis (NEB).

666 **Recombinant protein expression and purification.**

667 *Epitope scaffolds.*

668 Plasmids encoding epitope scaffolds were transformed into E. coli BL-21 (DE3) (New
669 England Biolabs) cells and 5mL starter cultures were grown overnight at 37C in Lysogeny Broth
670 (LB) supplemented with 50µg/mL kanamycin. The cultures were diluted 1:100 in Terrific BrothTB
671 media (RPI) supplemented with kanamycin and grown at 37 °C to an OD600 of ~0.6. The
672 temperature was subsequently lowered to 16 °C and the cultures were grown to OD600 of ~0.8
673 and induced with isopropyl β-D-1-thiogalactopyranoside (IPTG) to a final concentration of 0.5mM.
674 The cultures were shaken for 16–18 hours at 200rpm. Cell pellets were collected by centrifugation
675 at 14,500x*g*xg and lysed in B-PER Reagent (ThermoFisher Scientific) according to the
676 manufacturer's protocol. The lysates were centrifuged at 14,000 xg for 30 minutes at 4C. The
677 supernatant was incubated with Ni-NTA beads (Qiagen) equilibrated with native binding buffer
678 (20mM NaH2PO4, 500M NaCl, 2% glycerol, 10mM imidazole, pH=7.5) for an hour at 4C. The
679 beads were settled by centrifugation and the supernatant was removed by pipetting. The beads
680 were washed with wash buffer (50mM NaH2PO4, 500M NaCl, 2% glycerol, 30mM imidazole,
681 pH=7.5) after which the protein was eluted with elution buffer (20mM NaH2PO4, 500M NaCl,
682 250mM imidazole, pH=7.5). Protein expression and purity was confirmed by SDS-PAGE analysis,
683 and quantified spectrophotochemically at 280nm on a Nanodrop 2000 (ThermoFisher Scientific).
684 The eluted protein was concentrated on 3kDa MW spinMW spin columns (ThermoFisher
685 Scientific) and further purified by size exclusion chromatography in 20mM NaH2PO4, 150mM
686 NaCl, pH=7.5, on an AKTA-Go FPLC (Cytiva) using a Superdex 200 Increase 10/300GL column.
687 Fractions containing monomeric protein were pooled and concentrated as above.

688 *Monoclonal antibodies.*

689 Expi293F cells (ThermoFisher Scientific) were split to a density of $2.5x10^6$ cells/mL in
690 Expi293 Expression Medium with GlutaMAX (Gibco) and were transiently transfected with an
691 equimolar plasmid mixture of heavy and light chain using Expifectamine (Invitrogen). For a typical
692 100mL size transfection 100µg amount of total DNA and 270µL of lipofectamine were used. After

693 overnight incubation, enhancers were added as per the manufacturer's protocol and the cultures
694 were incubated with shaking for five days at 37C and 5% CO_2. The cell culture was centrifuged
695 to remove the cells and the supernatant was filtered with a 0.8-micron filter. The filtered
696 supernatant was incubated with equilibrated Protein A beads (ThermoFisher) for one hour at 4 °C
697 and washed with 20mM Tris, 350mM NaCl at pH=7. The antibodies were eluted with a 2.5%
698 Glacial Acetic Acid Elution Buffer and were buffer exchanged into 25mM Citric Acid, 125mM NaCl
699 buffer at pH=6. IgG expression was confirmed by reducing SDS-PAGE and quantified by
700 measuring absorbance at 280nmm (Nanodrop 2000).

701 **Antigenic characterization of epitope-scaffolds.**

702 *Binding by Surface Plasmon Resonance.*

703 To determine the dissociation constants (K_Ds) between epitope scaffolds and target
704 antibodies, binding was measured by Surface Plasmon Resonance (SPR) on a Biacore T200
705 instrument using Protein-A coated S series chips. The target antibodies were individually captured
706 for 60 sec at 30 µL/min to a level of 1000-2000RU onto this surface. The epitope scaffolds were
707 subsequently injected as analytes at five concentrations using the single cycle injection method.
708 The association phase was carried out for 180 seconds and the dissociation was done for 900
709 seconds with HBS-EP+ buffer flowing at 30µL/min. Regeneration of the binding surface was done
710 in 10mM glycine-HC, pH=2 for 30 seconds at 30µL/min with a 30 second baseline stabilization. A
711 1:1 Langmuir or Heterogenous ligand model was used for data fitting and analysis. For K_Ds
712 between Spike proteins and target antibodies, neutravidin (Thermo Scientific) was first captured
713 for 30-60 sec at 30 µL/min to a level of 1000-2000RU using CM5 S-series chips. Then biotinylated
714 Spike proteins (WA-2, 2P, R&D systems) were subsequently captured to a level of 3-500RU by
715 the neutravidin. FAB fragments of antibodies were then injected as analytes at five concentrations
716 using the single cycle method described above.

717 *Antibody binding by ELISA.*

718 Spike$^{815-823}$ peptide (residues 808-833) and stem helix (1140-1163) peptides and mutated
719 variants were commercially synthesized (Genscript). The following Spike proteins were used: WA-
720 2, 2P; SARS-CoV-1, 2P; MERS, 2P; OC43, 2P; HKU-1, 2P; GXP4L, 2P; SHC014, 2P; RaTG13,
721 2P, (all produced according to [38,39]); and Delta; BA1.1, Hexapro; XBB, Hexapro; 229E; NL63; (all
722 Sino Biological). Peptides and Spikes were diluted to 2µg/mL in 0.1M Sodium Bicarbonate and
723 epitope scaffolds were diluted to 100µg/mL. Antigens were coated onto 96 or 384 well high
724 binding enzyme-linked immunosorbent assay (ELISA) plates (Corning) by overnight incubation at
725 4C. Plates were washed with Superwash buffer (1X PBS supplemented with 0.1% Tween-20)
726 and blocked for 1 hour at room temperature with Superblock buffer supplemented with azide (80g
727 Whey Protein, 300mL Goat Serum, 20mL aqueous 5% Sodium Azide, 10mL Tween20, 80mL of
728 25X PBS, diluted to 2L). Antibodies starting at 100µg/mL were serially diluted in Superblock with
729 azide using a threefold serial dilution, added to the plates, and incubated at room temperature for
730 1 hour. Plates were then washed twice with Superwash and goat anti Human IgG-HRP secondary
731 antibody (Jackson Immunoresearch) diluted in SuperBlock (without Sodium azide) was
732 subsequently added. After incubating at room temperature for 1 hour, the plates were washed
733 four times in Superwash. Room temperature TMB (Tetramethylbenzidine) substrate was added
734 and after 5 minutes elapsed, the reaction was stopped by acid stop solution (0.33N HCl).
735 Absorption was measured at 405nm on a Cytation 1 plate reader (BioTek). Data was analyzed
736 and plotted with Prism version 10.0.0 (Graphpad).

737 *Sera binding by ELISA.*

738 Antigens were diluted to 2µg/mL in 0.1M Sodium Bicarbonate and coated onto 384 well
739 high binding enzyme-linked immunosorbent assay (ELISA) plates (Corning) by overnight
740 incubation at 4C. Plates were washed with Superwash buffer (1X PBS supplemented with 0.1%

741 Tween-20) and blocked for 1 hour at room temperature with Superblock buffer supplemented with
742 azide (80g Whey Protein, 300mL Goat Serum, 20mL aqueous 5% Sodium Azide, 10mL Tween20,
743 80mL of 25X PBS, diluted to 2L). Mouse sera starting at a dilution ratio of 1:50 and control
744 antibodies starting at 100µg/mL were serially diluted in Superblock with azide using a fivefold
745 serial dilution scheme. Human sera starting at a dilution ratio of 1:30 and control antibodies
746 starting at 100µg/mL were serially diluted in Superblock with azide using a threefold serial dilution
747 scheme. Sera and controls were added to the plates and incubated at room temperature for 1.5
748 hours. Plates were then washed twice with Superwash and the corresponding IgG-HRP
749 secondary antibody (goat anti mouse IgG-HRP or goat anti human IgG-HRP; Jackson
750 Immunoresearch) diluted in SuperBlock (without Sodium azide) was subsequently added. After
751 incubating at room temperature for 1 hour, the plates were washed four times in Superwash.
752 Room temperature TMB (Tetramethylbenzidine) substrate was added and after 15 minutes
753 elapsed, the reaction was stopped by acid stop solution (0.33N HCl). Absorption was measured
754 at 405nm on a SpectraMax Plus plate reader (Molecular Devices). Data was analyzed and plotted
755 with Prism version 10.0.0 (Graphpad).

756 **Structural analysis by x-ray crystallography.**

757 Crystallography experiments were performed using the sitting drop vapor diffusion
758 technique. 96-well crystallization plates were set, in which the protein of interest was mixed in a
759 1:1 ratio with reservoir solution. For *S2hlx-Ex*19, crystals were obtained when a 9.5mg/mL sample
760 was mixed with 0.1 M citric acid, 3.0 M sodium chloride, pH 3.5 (Index Screen) at 4℃. *S2hlx*-7
761 and antibody DH1057.1 were mixed in 1:1 molar ratio (300uM) and incubated for one hour at 4C.
762 Crystals for the complex were obtained in 25% PEG 3350 at room temperature. Prior to data
763 collection, crystals were cryoprotected in mother liquor supplemented with 20% glycerol before
764 being plunge-frozen into liquid nitrogen. A full description of the crystallographic data collection

765 and refinement statistics can be found in **Supplementary Table 2**. Diffraction data were indexed
766 in iMOSFLM[40] and scaled in AIMLESS[41]. Molecular replacement solutions for both *S2hlx-Ex*19
767 and the *S2hlx*-7-DH1057.1 complex were found in PhaserMR[42], using PDB ID: 3N1B as a search
768 ensemble for *S2hlx-Ex*19, PDB ID: 3LMO as a search ensemble for *S2hlx*-7 and PDB ID: 6UOE
769 as a search ensemble for DH1057.1. Coordinates for *S2hlx-Ex*19 and *S2hlx*-7-DH1057.1 were
770 iteratively built and refined using Coot[43], ISOLDE[44] and Phenix[45] to Rwork/Rfree values of 25.4/
771 27.5 and 21.1/24.5, respectively. The presence of translational non-crystallographic symmetry in
772 the *S2hlx*-7-DH1057.1 crystal likely accounts for its relatively high Rfree value and the L-test did
773 not indicate the presence of any twinning.

774 **Reactivity of designed epitope scaffolds with human samples.**

775 Human subject studies were approved by the Duke University Health System Institutional
776 Review Board (IRB) and conducted in agreement with the policies and protocols approved by the
777 Duke IRB, consistent with the Declaration of Helsinki. Written informed consent was obtained
778 from all research subjects or their legally authorized representatives. Study participants with
779 SARS-CoV-2 acute infection were enrolled in the Molecular and Epidemiological Study of
780 Suspected Infection protocol (MESSI, IRB Pro00100241) at Duke University, and were followed
781 longitudinally. Samples were selected for this study from participants who had seroconverted and
782 had symptom onset more than 10 days prior. From patient 26 and patient 29, PBMCs were
783 collected and analyzed by FACS at the same time point used for sera analysis for patient 26 and
784 7 days later for patient 29. Samples from vaccinated only participants were obtained from subjects
785 enrolled in the Study of Immune Response to COVID-19 Vaccines (IRB Pro00107929) at Duke
786 University. Supplementary Table 2 describes the vaccination protocol, SARS-CoV-2 variant
787 detected and the time of collection for the samples used in this analysis.

788 Human sera was analyzed as described above in *sera binding by ELISA* method.
789 Statistical differences were tested using the Wilcoxon signed rank test.

790 **Isolation and analysis of epitope scaffold reactive B cells.**

791 We prepared B cell tetramers of biotinylated S2hlx-Ex19 or FP-10 by mixing with
792 Streptavidin-VB515 (Miltenyi Biotec) and Streptavidin-AlexaFluor 647 (ThermoFisher Scientific)
793 at 4:1 molar ratio. A scaffold-only tetramer was also made with biotinylated S2hlx-Ex19-PShlx or
794 FP-10-wt mixed with Streptavidin-BV421 (Biolegend). These probes did not contain the grafted
795 epitope.

796 Cryopreserved PBMCs were thawed in warm RPMI-1640 containing 10% FBS, then
797 counted. Cells were stained with pre-optimized concentrations of the following antibodies: PE
798 anti-human IgD (clone IA6-2, BD Biosciences), PE-TXRD anti-human CD10 (clone HI10A, BD
799 Biosciences), PE-Cy5 anti-human CD3 (clone HIT3a, BD Biosciences), PE-Cy7 anti-human C27
800 (clone O323, ThermoFisher Scientific), AlexaFluor 700 anti-human CD38 (clone LS198-4-3,
801 Beckman Coulter), APC-Cy7 anti-human CD19 (clone SJ25C1, BD Biosciences), BV570 anti-
802 human CD16 (clone 3G8, Biolegend), BV605 anti-human CD14 (clone M5E2, Biolegend), and
803 BV711 anti-human IgM (clone G20-127, BD Biosciences). S2hlx-Ex19-VB515- and -AF647, and
804 S2hlx-Ex19-PShlx-BV421 were added to identify stem helix epitope-specific B cells. Cells were
805 incubated with Aqua Live/Dead (ThermoFisher Scientific) to exclude dead cells. Cells were
806 acquired on a BD S6 cell sorter (BD Biosciences). Data were analyzed using FlowJo v10.8 (BD
807 Biosciences).

808 Immunoglobulin heavy and light chain variable regions (VH and VK/L) from singly sorted
809 antigen-specific memory B cells were RT-PCR amplified using SuperScript III and AmpliTaq Gold
810 360 Master Mix (Thermo Fisher Scientific, Waltham, MA) under conditions previously described[46].

811 PCR products were purified in Biomek FX Laboratory Automation Workstation (Beckman Coulter,
812 Indianapolis, IN) and sequenced by Sanger sequencing. The V(D)J rearrangement, somatic
813 hypermutation frequency, CDR3 length of VH and VK/L chains, and antibody clonal lineages were
814 analyzed using the software Cloanalyst[47]. The heavy chains of mAbs DH1493, DH1501, and
815 DH1502 were assigned to the same clone by the software package Cloanalyst. Unmutated
816 common ancestor (UCA) inference was performed using the heavy and kappa chain pairs of the
817 three mAbs using the paired-chain inference implementation of the UCA inference part of the
818 software package Cloanalyst.

819 RT-PCR amplified sequences were transiently expressed as previously described[24].
820 Briefly, the linear expression cassettes were constructed by overlapping PCR to place the PCR-
821 amplified VH and VK/L chain genes under the control of a CMV promoter along with heavy chain
822 IgG1 constant region or light chain constant region and a BGH ploy A signal sequence. The linear
823 expression cassettes of heavy and light chains were then co-transfected into 293T cells in 6-well
824 plates. After 3 days, the cell culture supernatants were harvested and concentrated for binding
825 assays. For antibodies of interest, recombinant IgG1 monoclonals were expressed and purified
826 as described above.

827 **Pseudovirus neutralization assay.**

828 The pseudovirus neutralization assay performed at Duke has been described in detail[48]
829 and is a formally validated adaptation of the assay utilized by the Vaccine Research Center; the
830 Duke assay is FDA approved for D614G and other SARS-CoV-2 variants. For measurements of
831 neutralization, pseudovirus was incubated with 8 serial 5-fold dilutions of antibody samples in
832 duplicate in a total volume of 150 µl for 1 hr at 37C in 96-well flat-bottom culture plates.
833 293T/ACE2-MF cells were detached from T75 culture flasks using TrypLE Select Enzyme
834 solution, suspended in growth medium (100,000 cells/ml) and immediately added to all wells

835 (10,000 cells in 100 µL of growth medium per well). One set of 8 wells received cells + virus (virus
836 control) and another set of 8 wells received cells only (background control). After 71-73 hrs of
837 incubation, medium was removed by gentle aspiration and 30 µl of Promega 1X lysis buffer was
838 added to all wells. After a 10-minute incubation at room temperature, 100 µl of Bright-Glo
839 luciferase reagent was added to all wells. After 1-2 minutes, 110 µl of the cell lysate was
840 transferred to a black/white plate. Luminescence was measured using a GloMax Navigator
841 luminometer (Promega). Neutralization titers are the inhibitory dilution (ID) of serum samples at
842 which RLUs were reduced by 50% (ID50) compared to virus control wells after subtraction of
843 background RLUs. Serum samples were heat-inactivated for 30 minutes at 56C prior to assay.

844 **Infected-cell antibody binding assay.**

845 The binding of isolated anti-SARS-CoV-2 monoclonal antibodies to infected cells was
846 measured as previously reported[49]. Briefly, Vero E6 cells expressing TMPRSS2 and ACE2 and
847 infected with either D614G (Germany/BavPat1/2020) or BA.1 (hCoV-19/USA/MD-
848 HP20874/2021) variants were incubated with TrypLE Select (Gibco) for 15 minutes at 37°C to
849 detach cells and washed with PBS. Monoclonal antibodies were then added to infected cells at 2,
850 10 or 50 µg/mL. Approximately $2x10^5$ infected cells were incubated with the mAbs for 30 minutes
851 at room temperature, washed and then incubated with vital dye (Live/Dead Far Red Dead Cell
852 Stain, Invitrogen) for 15 minutes at room temperature to exclude nonviable cells from subsequent
853 analysis. Cells were then washed with Wash Buffer (1%FBS-PBS; WB), pelleted by centrifugation
854 and incubated with 1 mL of 4% Methanol-free Formaldehyde (Duke GHRB SOP 38; Attachment
855 17) for 30 minutes at room temperature. Cells were then washed twice with Wash Buffer,
856 permeabilized with CytoFix/CytoPerm (BD Biosciences) and stained with A568-conjugated anti-
857 SARS-COV-2 nucleocapsid antibody (40143-MM08, Sino Biological) and PE/Cy7-conjugated
858 secondary anti-Human IgG Fc antibody (Clone: HP6017, Biolegend) for 30 minutes at room
859 temperature. Cells were washed and resuspended in 250 µL PBS–1% paraformaldehyde.

860 Samples were acquired within 24 h using a BD Fortessa cytometer and a High Throughput
861 Sampler (HTS, BD Biosciences). Data analysis was performed using FlowJo 10 software (BD
862 Biosciences). Gates were set to include singlet, live, nucleocapsid+ (NC+) and IgG+ events.
863 Binding to mock infected cells was measured using the live cell gate as there were no NC+ events.
864 All final data represent specific binding, determined by subtraction of non-specific binding
865 observed in assays performed with mock-infected cells.

866 **Antibody-dependent NK cell degranulation assays (infected and Spike-transfected).**

867 Cell-surface expression of CD107a was used as a marker for NK cell degranulation and
868 performed as previously described[49]. Briefly, target cells were 293T cells 2-days post transfection
869 with a SARS-CoV-2 S protein (D614G) expression plasmid. Natural killer cells purified by negative
870 selection (Miltenyi Biotech) from peripheral blood mononuclear cells obtained by leukapheresis
871 from a healthy, SARS-CoV-2-seronegative individual (Fc-gamma-receptor IIIA (Fcy-RIIIA)158
872 V/F heterozygous) previously assessed for Fcy-RIIIA genotype and frequency of NK cells were
873 used as a source of effector cells. NK cells were incubated with target cells at a 1:1 ratio in the
874 presence of monoclonal antibodies, Brefeldin A (GolgiPlug, 1 µl/ml, BD Biosciences), monensin
875 (GolgiStop, 4µl/6mL, BD Biosciences), and anti-CD107a-FITC (BD Biosciences, clone H4A3) in
876 96-well flat bottom plates for 6 hours at 37ºC and 5% CO_2. NK cells were removed from the wells
877 and stained for viability prior to staining with CD56-PECy7 (BD Biosciences, clone NCAM16.2),
878 CD16-PacBlue (BD Biosciences, clone 3G8), and CD69-BV785 (Biolegend, Clone FN50). After
879 three washes, cells were resuspended in 115 µL PBS–1% paraformaldehyde. Flow cytometry
880 data analysis was performed using FlowJo software (v10). Data is reported as the area under the
881 curve (AUC) of %CD107a+ live NK cells (gates included singlets, lymphocytes, aqua blue-,
882 CD56+ and/or CD16+, CD107a+), calculated as previously described[49] at three concentrations of
883 monoclonal antibody: 2, 10 and 50 µg/mL. All final data represent specific activity, determined by
884 subtraction of non-specific activity observed in assays performed with mock-infected cells and in

885 the absence of antibodies, and in the presence of a non-specific monoclonal antibody, the anti-
886 HIV-1 antibody VRC01.

887 **Development of mi03 nanoparticles conjugated with epitope scaffolds for immunizations.**

888 *SpyCatcher003-Mi3 Nanoparticles.*

889 Plasmid encoding for the spycatcher003-mi3 particles was acquired from Addgene
890 (Plasmid #159995) and transformed into *E. coli* BL-21 (RIPL) (Agilent Technologies) cells. Five
891 milliliters starter cultures were grown overnight at 37C in Lysogeny Broth (LB) supplemented with
892 1% glucose and 50µg/mL kanamycin. Cultures were diluted 1:100 in Terrific Broth (TB) media
893 (RPI) supplemented with kanamycin and grown at 37C to an OD_{600} of ~0.6. The temperature was
894 subsequently lowered to 20C and the cultures were grown to OD_{600} of ~0.8 and induced with
895 isopropyl β-D-1-thiogalactopyranoside (IPTG) to a final concentration of 0.5mM. The cultures
896 were shaken for 16–18 hours at 250rpm. Cell pellets were collected by centrifugation at 6,000xg
897 and the pellets were stored overnight at -20C. Pellets were resuspended in 40 mL of 25mM Tris-
898 HCl, 300mM NaCl, pH=8.5 supplemented with a working concentration of 2mM PMSF dissolved
899 in isopropanol, 40mg lysozyme (0.1mg/mL) and 1 tablet of protease inhibitor. The lysates were
900 incubated at room temperature for 30 minutes on a platform shaker and later sonicated for 13
901 minutes with 10s on and 30s off 50% duty-cycle. The sonicated lysates were centrifuged for 45
902 minutes at 18,000xg at 4C. To precipitate the spycatcher003-mi3 nanoparticles, 170 mg/mL of
903 ammonium sulfate was added to the supernatant solution and subsequently shaken at 4C for 1
904 hour. Precipitated particles were collected by centrifuging at 16,000xg for 30 minutes at 4C. The
905 supernatant was discarded, and the pellet was washed with endotoxin-free water to remove
906 residual salty buffer. The nanoparticles were resolubilized in 8mL of 25mM Tris-HCl, 150mM
907 NaCl, pH=8.5. To remove insoluble aggregates, the solubilized nanoparticles were centrifuged at
908 18,000xg for 30 minutes. Nanoparticle expression and purity was confirmed by SDS-PAGE

909 analysis, and quantified spectrophotochemically at 280nm on a Nanodrop 2000 (ThermoFisher
910 Scientific). The spycatcher003-mi3 nanoparticles were concentrated in a 10kDa MW spin columns
911 (ThermoFisher Scientific) and further purified by size exclusion chromatography in 25mM Tris,
912 150mM NaCl, pH=8.0, on an AKTA-Go FPLC (Cytiva) using a Superose 6 Increase 10/300GL
913 column. Fractions containing the spycatcher003-mi3 nanoparticles were pooled and concentrated
914 as above. The nanoparticles were stored at -80C.

915 *Conjugation of epitope scaffolds to Spycatcher003-mi3 nanoparticles.*

916 Epitope scaffolds were mixed with spycatcher003-mi3 nanoparticles in a 1.2:1 molar ratio.
917 The complex was mixed thoroughly and incubated overnight on ice at 4C. Conjugation was
918 confirmed by SDS-PAGE. The conjugated nanoparticles were separated from excess monomeric
919 epitope scaffolds by size-exclusion chromatography in 25mM Tris, 150mM NaCl, pH 8.0, on an
920 AKTA-Go FPLC (Cytiva) using a Superose 6 Increase 10/300GL column. Fractions containing
921 the epitope-scaffold-mi3 nanoparticles were pooled and concentrated as above. Endotoxins were
922 removed by treating the nanoparticles with 2% triton X-100 as previously described[50]. Endotoxin
923 levels were tested by a chromogenic endotoxin quantification kit (ThermoFisher Scientific). The
924 endotoxin-free nanoparticles were stored at -80C.

925 Nanoparticles were analyzed by Negative Stain Electron Microscopy to confirm that they
926 were well formed. A frozen aliquot was thawed in RT water bath, then placed on ice. The sample
927 was then diluted to 400 µg/ml with 5 g/dl Glycerol in HBS (20 mM HEPES, 150 mM NaCl pH 7.4)
928 buffer containing 8 mM glutaraldehyde. After 5 min incubation, glutaraldehyde was quenched by
929 adding sufficient 1 M Tris stock, pH 7.4, to give 80 mM final Tris concentration and incubated for
930 5 min. Quenched sample was applied to a glow-discharged carbon-coated EM grid for 10-12
931 second, then blotted, and stained with 2 g/dL uranyl formate for 1 min, blotted and air-dried. Grids
932 were examined on a Philips EM420 electron microscope operating at 120 kV and nominal

933 magnification of 49,000x, and 30 images were collected on a 76 Mpix CCD camera at 2.4
934 Å/pixel. Images were analyzed by 2D and 3D class averages using standard protocols with Relion
935 3.0[51].

936 **Mouse immunization and protection studies.**

937 *Immunization studies in BALB/c mice.*

938 BALB/c (#028) female mice were purchased from Charles River. The Toll-like receptor 4
939 agonist glucopyranosyl lipid adjuvant–stable emulsion (GLA-SE) was used as the adjuvant for the
940 vaccine immunogens. Groups of mice (n=8) were vaccinates intramuscularly with GLA-SE-
941 adjuvanted Ex15-NP; GLA-SE-adjuvanted Ex_mosaic-NP; GLA-SE-adjuvanted mixture of equal
942 parts Ex15-NP, Ex17_NP, Ex19_NP and Ex20_NP; or GLA-SE-adjuvanted Ex15-NP (prime),
943 followed by Ex19_NP (boost 1) and Ex20_NP (boost 2). An adjuvant-only group (n=4) was
944 included for comparison. Vaccine immunogens were administered at 5μg and formulated with 5μg
945 of adjuvant. Mice were immunized at week 0, week 4 , and week 8. Blood samples were collected
946 either 7 days prior to immunization (pre-bleed), or 7 days after each immunization. Seven days
947 after the final dose mice were sacrificed for terminal analysis.

948 *Live virus protection studies.*

949 Nineteen to twenty-one female k18-hACE2 mice purchased from Jackson Laboratory
950 (B6.Cg-Tg(K18-ACE2)2Prlmn/J; JAX strain number #034860) were used for the WIV-1 viral
951 challenge studies. The Toll-like receptor 4 agonist glucopyranosyl lipid adjuvant–stable emulsion
952 (GLA-SE) was used as the adjuvant for the vaccine immunogens. Mouse vaccination studies
953 were performed intramuscularly twice with mRNA ACLNP 307 2019NCOV WUHAN S-2P spike
954 followed by two additional shots of either mRNA spike or GLA-SE-adjuvanted Ex_mosaic-NP.
955 Protein immunogens were administered at 10μg formulated with 5μg of adjuvant. mRNA

956 immunogens were administered at 20µg. Mice were immunized at week 0, week 4, week 8, and
957 week 12. Blood samples were collected either 7 days prior to immunization (pre-bleed), or 7 days
958 after each immunization. Mice were then moved into the BSL3 and acclimated. For infection,
959 vaccinated mice were anaesthetized with ketamine/xylazine and infected with 1 x 10^4 PFU WIV1-
960 CoV intranasally in a total volume of 50ul[52]. Infected mice were weighed daily.

961 Mouse studies were performed according to the recommendations for the care and use of
962 animals by the Office of Laboratory Animal Welfare (OLAW), National Institutes of Health, and
963 the Institutional Animal Care and Use Committee (IACUC) at the University of North Carolina
964 (UNC permit no. A-3410-01). All infectious work was performed in Biosafety Level 3 laboratories
965 (BSL-3) with approved standard operating procedures and safety conditions for SARS-CoV-2.

966 For virus titration by plaque assay, the caudal lobe of the right lung was homogenized in
967 phosphate-buffered saline (PBS), and the homogenate was serial diluted and inoculated onto
968 Vero E6 cells [American Type Culture Collection (ATCC), CRL1586], followed by agarose overlay.
969 Plaques were visualized with an overlay of neutral red dye on day 2 after infection. At indicated
970 time points, mice were euthanized and gross pathology (congestion score) of the lung tissue was
971 assessed and scored on a scale from 0 (no lung congestion) to 4 (severe congestion affecting all
972 lung lobes).

973

974

975

976

977

978 ## References

979 1 Piccoli, L. *et al.* Mapping Neutralizing and Immunodominant Sites on the SARS-CoV-2
980 Spike Receptor-Binding Domain by Structure-Guided High-Resolution Serology. *Cell* **183**,
981 1024-1042 e1021 (2020). https://doi.org:10.1016/j.cell.2020.09.037

982 2 Wang, Z. *et al.* mRNA vaccine-elicited antibodies to SARS-CoV-2 and circulating variants.
983 *Nature* **592**, 616-622 (2021). https://doi.org:10.1038/s41586-021-03324-6

984 3 Goel, R. R. *et al.* Distinct antibody and memory B cell responses in SARS-CoV-2 naïve and
985 recovered individuals after mRNA vaccination. *Science Immunology* **6**, eabi6950 (2021).
986 https://doi.org:10.1126/sciimmunol.abi6950

987 4 Robbiani, D. F. *et al.* Convergent antibody responses to SARS-CoV-2 in convalescent
988 individuals. *Nature* **584**, 437-442 (2020). https://doi.org:10.1038/s41586-020-2456-9

989 5 Starr, T. N. *et al.* Deep mutational scans for ACE2 binding, RBD expression, and antibody
990 escape in the SARS-CoV-2 Omicron BA.1 and BA.2 receptor-binding domains. *PLoS Pathog*
991 **18**, e1010951 (2022). https://doi.org:10.1371/journal.ppat.1010951

992 6 Qu, P. *et al.* Enhanced neutralization resistance of SARS-CoV-2 Omicron subvariants BQ.1,
993 BQ.1.1, BA.4.6, BF.7, and BA.2.75.2. *Cell Host Microbe* (2022).
994 https://doi.org:10.1016/j.chom.2022.11.012

995 7 Dacon, C. *et al.* Broadly neutralizing antibodies target the coronavirus fusion peptide.
996 *Science* **377**, 728-735 (2022). https://doi.org:10.1126/science.abq3773

997 8 Low, J. S. *et al.* ACE2-binding exposes the SARS-CoV-2 fusion peptide to broadly
998 neutralizing coronavirus antibodies. *Science* **377**, 735-742 (2022).
999 https://doi.org:10.1126/science.abq2679

1000 9 Pinto, D. *et al.* Broad betacoronavirus neutralization by a stem helix–specific human
1001 antibody. *Science* **373**, 1109-1116 (2021). https://doi.org:10.1126/science.abj3321

1002 10 Zhou, P. *et al.* A human antibody reveals a conserved site on beta-coronavirus spike
1003 proteins and confers protection against SARS-CoV-2 infection. *Science Translational*
1004 *Medicine* **14**, eabi9215 (2022). https://doi.org:10.1126/scitranslmed.abi9215

1005 11 Gobeil, S. M.-C. *et al.* Structural diversity of the SARS-CoV-2 Omicron spike. *Molecular Cell*
1006 **82**, 2050-2068.e2056 (2022). https://doi.org:10.1016/j.molcel.2022.03.028

1007 12 Stalls, V. *et al.* Cryo-EM structures of SARS-CoV-2 Omicron BA.2 spike. *Cell Reports* **39**,
1008 111009 (2022). https://doi.org:10.1016/j.celrep.2022.111009

1009 13 Dacon, C. *et al.* Rare, convergent antibodies targeting the stem helix broadly neutralize
1010 diverse betacoronaviruses. *Cell Host & Microbe* **0** (2022).
1011 https://doi.org:10.1016/j.chom.2022.10.010

1012 14 Zhou, P. *et al.* Broadly neutralizing anti-S2 antibodies protect against all three human
1013 betacoronaviruses that cause severe disease. (Immunology, 2022).

1014 15 Azoitei, M. L. *et al.* Computation-guided backbone grafting of a discontinuous motif onto
1015 a protein scaffold. *Science* **334**, 373-376 (2011). https://doi.org:10.1126/science.1209368

1016 16 Correia, B. E. *et al.* Computational Design of Epitope-Scaffolds Allows Induction of
1017 Antibodies Specific for a Poorly Immunogenic HIV Vaccine Epitope. *Structure* **18**, 1116-
1018 1126 (2010). https://doi.org:10.1016/j.str.2010.06.010

1019 17 Ofek, G. *et al.* Elicitation of structure-specific antibodies by epitope scaffolds. *Proceedings*
1020 *of the National Academy of Sciences* **107**, 17880-17887 (2010).
1021 https://doi.org:10.1073/pnas.1004728107

1022 18 Ofek, G. *et al.* Elicitation of structure-specific antibodies by epitope scaffolds. *Proc Natl*
1023 *Acad Sci U S A* **107**, 17880-17887 (2010). https://doi.org:10.1073/pnas.1004728107

1024 19 Sesterhenn, F. *et al.* Trivalent cocktail of de novo designed immunogens
1025 enables the robust induction and focusing of functional antibodies in vivo.
1026 *bioRxiv*, 685867 (2019). https://doi.org:10.1101/685867

1027 20 Li, D. *et al.* In vitro and in vivo functions of SARS-CoV-2 infection-enhancing and
1028 neutralizing antibodies. *Cell* **184**, 4203-4219.e4232 (2021).
1029 https://doi.org:10.1016/j.cell.2021.06.021

1030 21 Jumper, J. *et al.* Highly accurate protein structure prediction with AlphaFold. *Nature* **596**,
1031 583-589 (2021). https://doi.org:10.1038/s41586-021-03819-2

1032 22 Dauparas, J. *et al.* Robust deep learning–based protein sequence design using
1033 ProteinMPNN. *Science* **378**, 49-56 (2022). https://doi.org:10.1126/science.add2187

1034 23 Dacon, C. *et al.* Rare, convergent antibodies targeting the stem helix broadly neutralize
1035 diverse betacoronaviruses. *Cell Host & Microbe*
1036 https://doi.org:10.1016/j.chom.2022.10.010

1037 24 Liao, H.-X. *et al.* High-throughput isolation of immunoglobulin genes from single human B
1038 cells and expression as monoclonal antibodies. *Journal of Virological Methods* **158**, 171-
1039 179 (2009). https://doi.org:https://doi.org/10.1016/j.jviromet.2009.02.014

1040 25 Bruun, T. U. J., Andersson, A.-M. C., Draper, S. J. & Howarth, M. Engineering a Rugged
1041 Nanoscaffold To Enhance Plug-and-Display Vaccination. *ACS Nano* **12**, 8855-8866 (2018).
1042 https://doi.org:10.1021/acsnano.8b02805

1043 26 Saunders, K. O. *et al.* Neutralizing antibody vaccine for pandemic and pre-emergent
1044 coronaviruses. *Nature* **594**, 553-559 (2021). https://doi.org:10.1038/s41586-021-03594-
1045 0

1046 27 Shah, P., Canziani, G. A., Carter, E. P. & Chaiken, I. The Case for S2: The Potential Benefits
1047 of the S2 Subunit of the SARS-CoV-2 Spike Protein as an Immunogen in Fighting the
1048 COVID-19 Pandemic. *Frontiers in Immunology* **12** (2021).
1049 https://doi.org:10.3389/fimmu.2021.637651

1050 28 Azoitei, M. L. *et al.* Computational design of high-affinity epitope scaffolds by backbone
1051 grafting of a linear epitope. *J Mol Biol* **415**, 175-192 (2012).
1052 https://doi.org:10.1016/j.jmb.2011.10.003

1053 29 Dauparas, J. *et al.* Robust deep learning–based protein sequence design using
1054 ProteinMPNN. *Science* **378**, 49-56 (2022). https://doi.org:doi:10.1126/science.add2187

1055 30 Azoitei, M. L. *et al.* Computational design of protein antigens that interact with the CDR
1056 H3 loop of HIV broadly neutralizing antibody 2F5. *Proteins* **82**, 2770-2782 (2014).
1057 https://doi.org:10.1002/prot.24641

1058 31 Correia, B. E. *et al.* Computational design of epitope-scaffolds allows induction of
1059 antibodies specific for a poorly immunogenic HIV vaccine epitope. *Structure* **18**, 1116-
1060 1126 (2010). https://doi.org:10.1016/j.str.2010.06.010

1061 32 McLellan, J. S. *et al.* Design and characterization of epitope-scaffold immunogens that
1062 present the motavizumab epitope from respiratory syncytial virus. *J Mol Biol* **409**, 853-
1063 866 (2011). https://doi.org:10.1016/j.jmb.2011.04.044

1064 33 Correia, B. E. *et al.* Proof of principle for epitope-focused vaccine design. *Nature* **507**, 201-
1065 206 (2014). https://doi.org:10.1038/nature12966

1066 34 Jumper, J. *et al.* Highly accurate protein structure prediction with AlphaFold. *Nature* **596**,
1067 583-589 (2021). https://doi.org:10.1038/s41586-021-03819-2

1068 35 Havenar-Daughton, C. *et al.* The human naive B cell repertoire contains distinct subclasses
1069 for a germline-targeting HIV-1 vaccine immunogen. *Sci Transl Med* **10** (2018).
1070 https://doi.org:10.1126/scitranslmed.aat0381

1071 36 Leggat, D. J. *et al.* Vaccination induces HIV broadly neutralizing antibody precursors in
1072 humans. *Science* **378**, eadd6502 (2022). https://doi.org:doi:10.1126/science.add6502

1073 37 Zhou, P. *et al.* Broadly neutralizing anti-S2 antibodies protect against all three human
1074 betacoronaviruses that cause deadly disease. *Immunity* **56**, 669-686.e667 (2023).
1075 https://doi.org:10.1016/j.immuni.2023.02.005

1076 38 Li, D. *et al.* Breadth of SARS-CoV-2 neutralization and protection induced by a nanoparticle
1077 vaccine. *Nat Commun* **13**, 6309 (2022). https://doi.org:10.1038/s41467-022-33985-4

1078 39 Martinez, D. R. *et al.* A broadly cross-reactive antibody neutralizes and protects against
1079 sarbecovirus challenge in mice. *Sci Transl Med* **14**, eabj7125 (2022).
1080 https://doi.org:10.1126/scitranslmed.abj7125

1081 40 Battye, T. G., Kontogiannis, L., Johnson, O., Powell, H. R. & Leslie, A. G. iMOSFLM: a new
1082 graphical interface for diffraction-image processing with MOSFLM. *Acta Crystallogr D Biol*
1083 *Crystallogr* **67**, 271-281 (2011). https://doi.org:10.1107/S0907444910048675

1084 41 Evans, P. R. & Murshudov, G. N. How good are my data and what is the resolution? *Acta*
1085 *Crystallogr D Biol Crystallogr* **69**, 1204-1214 (2013).
1086 https://doi.org:10.1107/S0907444913000061

1087 42 McCoy, A. J. Solving structures of protein complexes by molecular replacement with
1088 Phaser. *Acta Crystallogr D Biol Crystallogr* **63**, 32-41 (2007).
1089 https://doi.org:10.1107/S0907444906045975

1090 43 Emsley, P. & Cowtan, K. Coot: model-building tools for molecular graphics. *Acta*
1091 *Crystallogr D Biol Crystallogr* **60**, 2126-2132 (2004).
1092 https://doi.org:10.1107/S0907444904019158

1093 44 Croll, T. I. ISOLDE: a physically realistic environment for model building into low-resolution
1094 electron-density maps. *Acta Crystallogr D Struct Biol* **74**, 519-530 (2018).
1095 https://doi.org:10.1107/S2059798318002425

1096 45 Adams, P. D. *et al.* PHENIX: a comprehensive Python-based system for macromolecular
1097 structure solution. *Acta Crystallogr D Biol Crystallogr* **66**, 213-221 (2010).
1098 https://doi.org:10.1107/S0907444909052925

1099 46 Liao, H. X. *et al.* High-throughput isolation of immunoglobulin genes from single human B
1100 cells and expression as monoclonal antibodies. *J Virol Methods* **158**, 171-179 (2009).
1101 https://doi.org:10.1016/j.jviromet.2009.02.014

1102 47 Kepler, T. B. *et al.* Reconstructing a B-Cell Clonal Lineage. II. Mutation, Selection, and
1103 Affinity Maturation. *Frontiers in Immunology* **5** (2014).
1104 https://doi.org:10.3389/fimmu.2014.00170

1105 48 Gilbert, P. B. *et al.* Immune correlates analysis of the mRNA-1273 COVID-19 vaccine
1106 efficacy clinical trial. *Science* **375**, 43-50 (2022).
1107 https://doi.org:doi:10.1126/science.abm3425

1108 49 Mielke, D. *et al.* Development of flow cytometry-based assays to assess the ability of
1109 antibodies to bind to SARS-CoV-2-infected and spike-transfected cells and mediate NK cell
1110 degranulation. *Cytometry A* **101**, 483-496 (2022). https://doi.org:10.1002/cyto.a.24552

1111 50 Teodorowicz, M. *et al.* Optimized Triton X-114 assisted lipopolysaccharide (LPS) removal
1112 method reveals the immunomodulatory effect of food proteins. *PLOS ONE* **12**, e0173778
1113 (2017). https://doi.org:10.1371/journal.pone.0173778

1114 51 Zivanov, J. *et al.* New tools for automated high-resolution cryo-EM structure
1115 determination in RELION-3. *eLife* **7**, e42166 (2018). https://doi.org:10.7554/eLife.42166

1116 52 Menachery, V. D. *et al.* SARS-like WIV1-CoV poised for human emergence. *Proceedings of*
1117 *the National Academy of Sciences* **113**, 3048-3053 (2016).
1118 https://doi.org:doi:10.1073/pnas.1517719113

1119

1120 **Figure1**

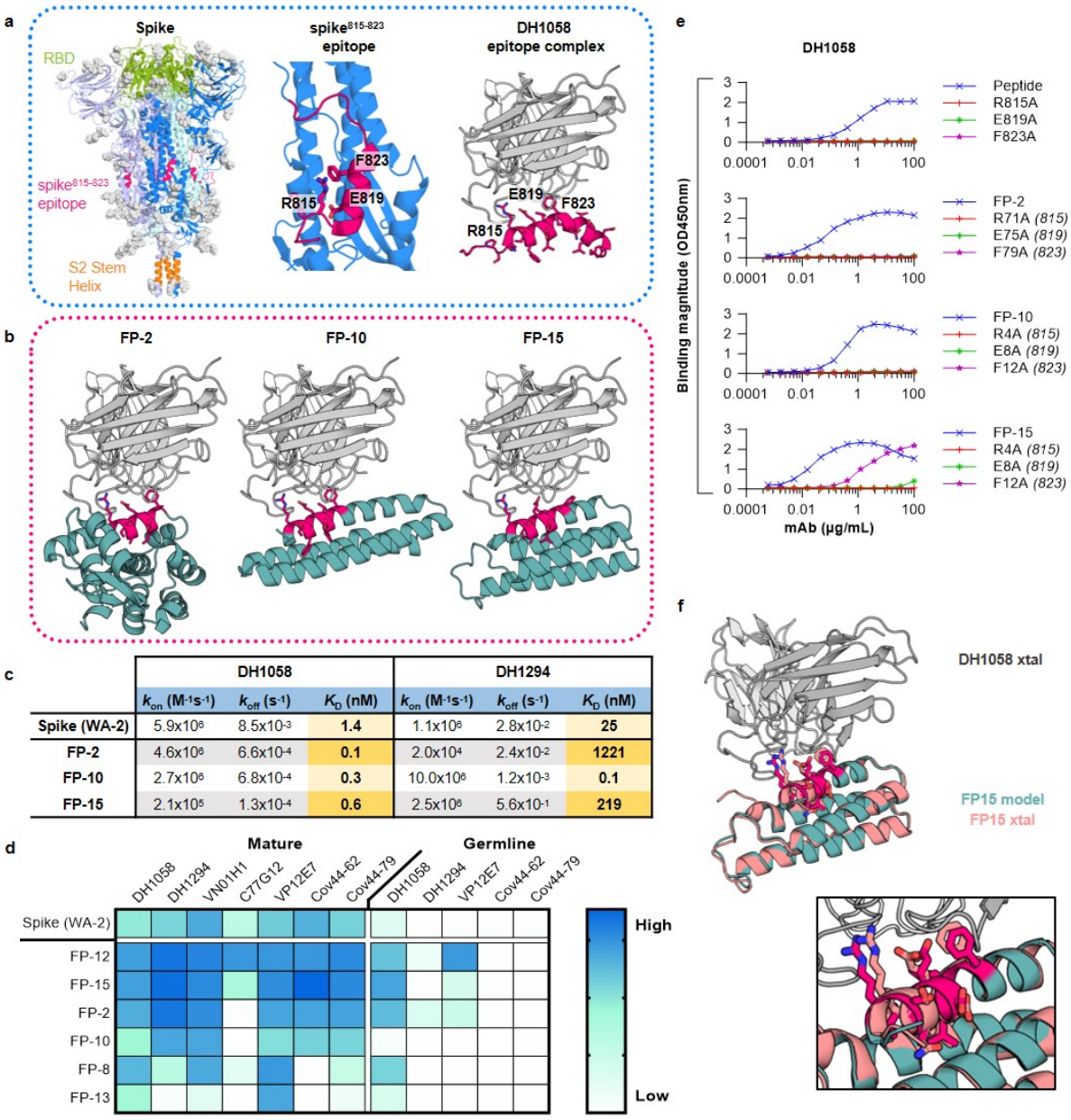

1121

1122 **Figure 1. Design of epitope scaffolds that bind to broadly cross-reactive antibodies against**

1123 **the spike$^{815-823}$ peptide. (a)** *Left*: Structure of the pre-fusion spike trimer (individual monomers:

1124 *blue, violet and pale green*; glycans: *grey*; PDBid:6xr8), with the RBD (*green*), spike$^{815-823}$ peptide

1125 (*red*) and stem helix (*orange*) domains highlighted. *Middle*: Zoom of spike monomer with spike^{815-}

1126 ^{823} peptide highlighted (*red*) showing key residues engaged by antibodies. *Right*: Structure of
1127 spike$^{815\text{-}823}$ peptide (*red*) bound to DH1058 mAb (*grey*) (PDBid:7tow). **(b)** Computational models
1128 of DH1058 (*grey*) bound to ESs FP-2, FP-10 and FP-15 (*green*) with the grafted epitope shown
1129 in *red sticks*. **(c)** Binding affinities of ESs and spike to DH1058 and DH1294 mAbs as determined
1130 by SPR. **(d)** Binding of spike and ES to diverse spike$^{815\text{-}823}$-targeting mAbs and their inferred
1131 precursors. **(e)** ELISA binding of DH1058 mAb to synthetic spike$^{815\text{-}823}$ peptides and
1132 representative ESs that contain alanine mutations at epitope residues critical for antibody
1133 recognition. Numbers in brackets indicate the equivalent position of the mutated epitope residues
1134 on spike. **(f)** Crystal structure of DH1058 mAb (*grey*) in complex with FP-15 (*salmon*) overlaid with
1135 the computational model of the ESs (*green*). Epitope residues are shown in sticks (model: *red*;
1136 crystal structure: *salmon*).

1137

1138 **Figure 2**

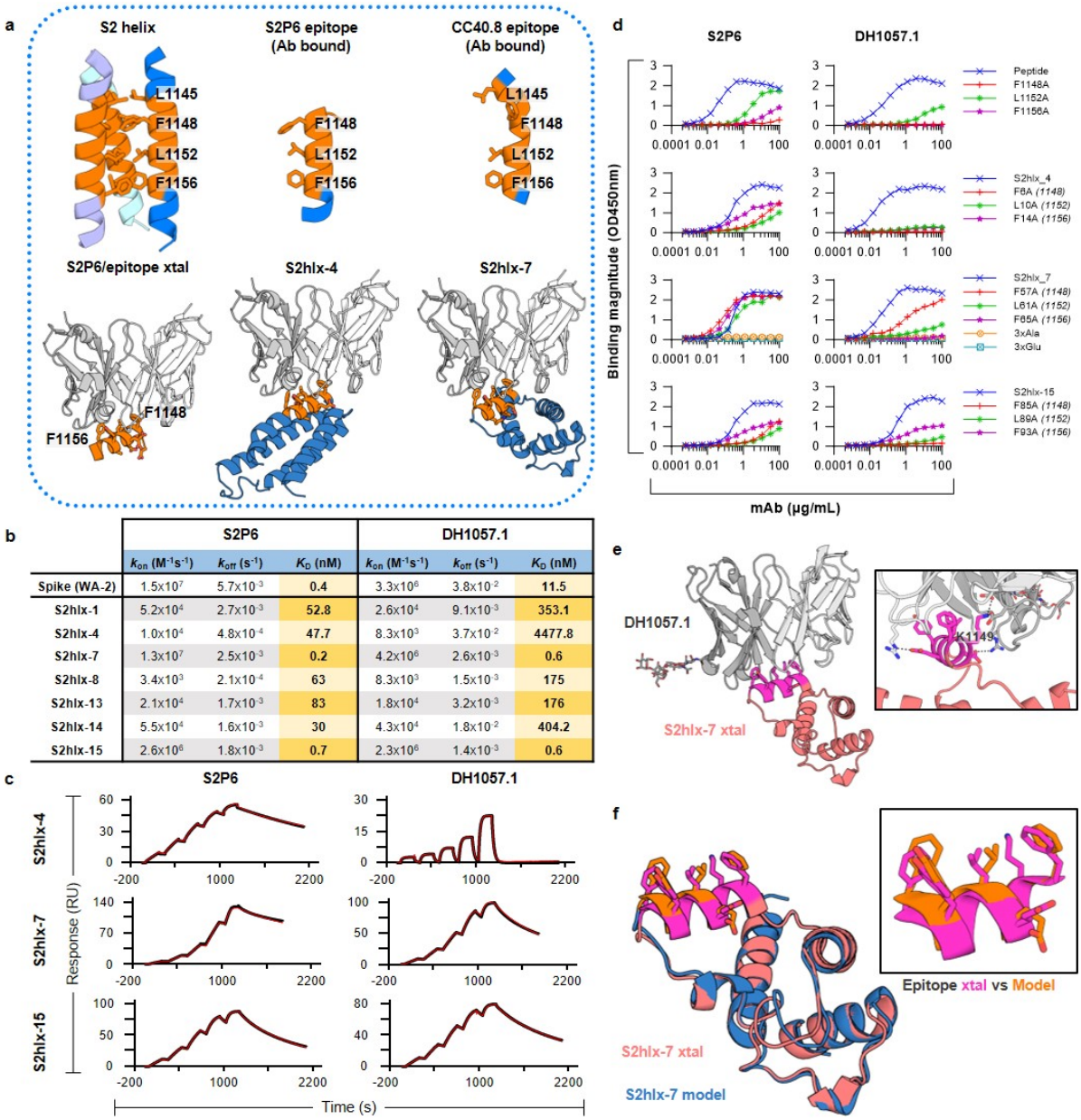

	S2P6			DH1057.1		
	k_{on} ($M^{-1}s^{-1}$)	k_{off} (s^{-1})	K_D (nM)	k_{on} ($M^{-1}s^{-1}$)	k_{off} (s^{-1})	K_D (nM)
Spike (WA-2)	$1.5x10^7$	$5.7x10^{-3}$	0.4	$3.3x10^6$	$3.8x10^{-2}$	11.5
S2hlx-1	$5.2x10^4$	$2.7x10^{-3}$	52.8	$2.6x10^4$	$9.1x10^{-3}$	353.1
S2hlx-4	$1.0x10^4$	$4.8x10^{-4}$	47.7	$8.3x10^3$	$3.7x10^{-2}$	4477.8
S2hlx-7	$1.3x10^7$	$2.5x10^{-3}$	0.2	$4.2x10^6$	$2.6x10^{-3}$	0.6
S2hlx-8	$3.4x10^3$	$2.1x10^{-4}$	63	$8.3x10^3$	$1.5x10^{-3}$	175
S2hlx-13	$2.1x10^4$	$1.7x10^{-3}$	83	$1.8x10^4$	$3.2x10^{-3}$	176
S2hlx-14	$5.5x10^4$	$1.6x10^{-3}$	30	$4.3x10^4$	$1.8x10^{-2}$	404.2
S2hlx-15	$2.6x10^6$	$1.8x10^{-3}$	0.7	$2.3x10^6$	$1.4x10^{-3}$	0.6

1139

1140 **Figure 2. Design of epitope scaffolds that bind to S2P6-like antibodies against the stem**
1141 **helix. (a)** The conformation of the stem helix epitope (*orange*) on the pre-fusion trimer, bound by
1142 S2P6 and CC40.8mAbs (PDBids:7rnj and 7sjs), and displayed on representative epitope
1143 scaffolds S2hlx-4 and -7. Key epitope residues are labeled and shown in sticks. **(b)** Binding

1144 affinities of spike and S2hlx ESs to S2P6 and DH1057.1 mAbs **(c)** Representative single-cycle
1145 binding SPR traces used to determine the dissociation constants in **(b)**. **(d)** The effect on S2P6
1146 and DH1057 mAbs binding to epitope mutations in synthesized stem helix peptides (1140-1164)
1147 and representative S2-hlx ESs. **(e)** Crystal structure of the DH1057.1 mAb (*grey*) bound to ES
1148 S2hlx-7 (*orange*) with the epitope in *pink sticks*. Inset shows details of the epitope/mAb
1149 interaction, with epitope residue K1149 highlighted. **(f)** Comparison of the S2hlx-7 conformation
1150 in the computational model (*pink*) and the crystal structure (*blue*), both overall and in the epitope
1151 region.

1152

1153 **Figure 3**

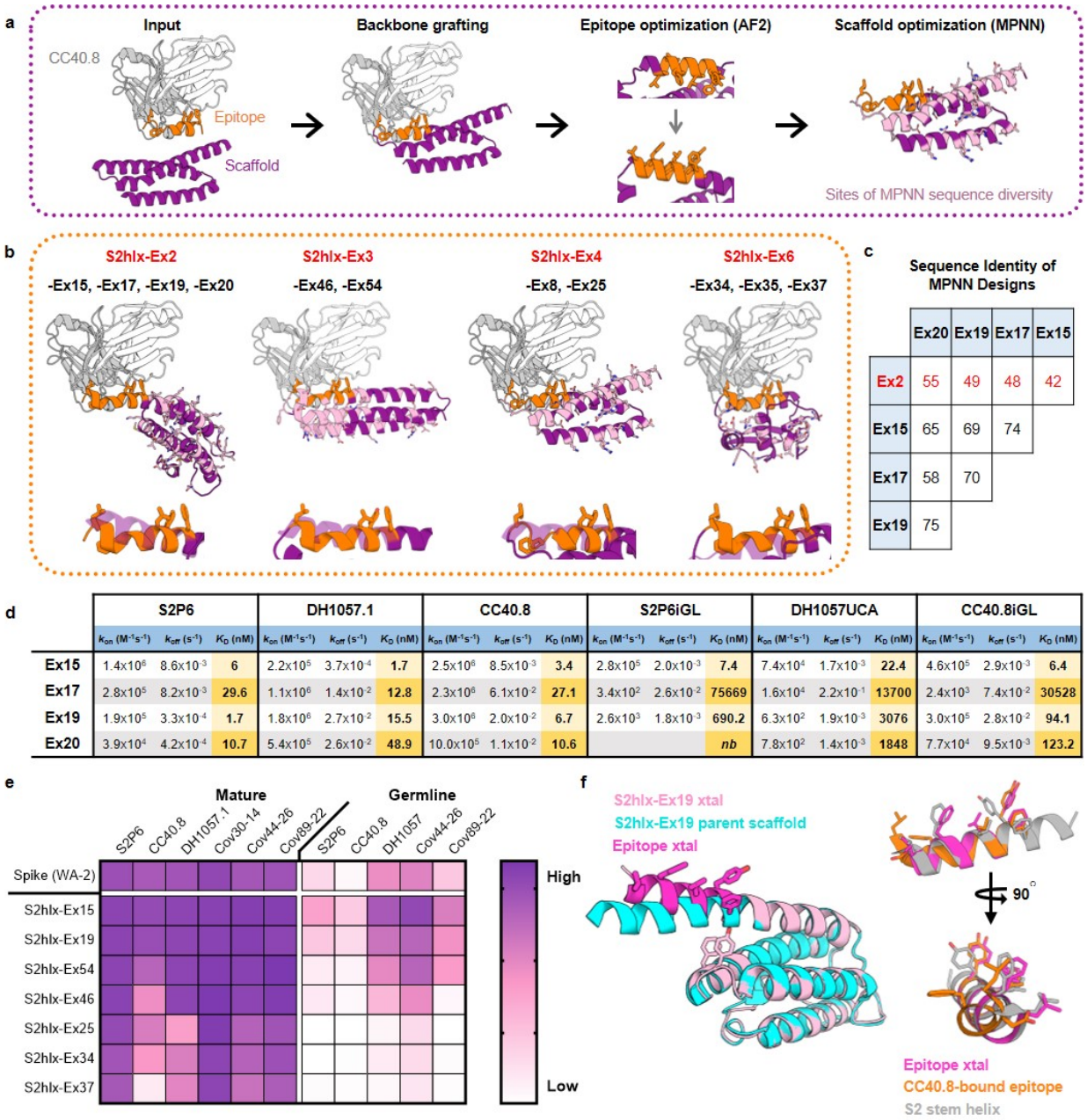

1154

1155 **Figure 3. Design of epitope scaffolds that engage two major classes of antibodies against**
1156 **the stem helix. (a)** Overview of the computational design process to graft the antibody-bound
1157 CC40.8 epitope onto candidate scaffolds. ESs were designed by transplanting the epitope
1158 backbone with Rosetta, validated with Alphafold2 and optimized for expression with

1159 ProteinMPNN. **(b)** *Top*: Computational models of CC40.8 mAb (*gray and white*) bound to ESs
1160 (*purple*) from the S2hlx-Ex2, S2hlx-Ex4, and S2hlx-Ex6 families of designs. The epitope is
1161 highlighted in *orange sticks*. Residues designed by ProteinMPNN and that can differ between
1162 designs from the same family are shown in *pink sticks*. *Bottom*: Overlay of the grafted epitope
1163 conformation (*orange*) and the parent scaffold structure it replaced (*purple*). **(c)** Sequence identity
1164 between S2hlx-Ex2 family of ESs designed by ProteinMPNN. **(d)** Dissociation constants of S2hlx-
1165 Ex2 based designs to S2P6, DH1057 and CC40.8 mAbs and their precursors. *nb*=not binding. **(e)**
1166 Binding of spike and S2hlx-Ex ESs to diverse stem helix mAbs and their precursors. **(f)** *Left*:
1167 alignment of the S2hlx-Ex19 parent scaffold (*cyan*) with the crystal structure of the unbound
1168 epitope scaffold (*pink*, with the epitope in *magenta sticks*). Residues Tyr62 and Phe66 that
1169 stabilize the grafted epitope conformation are highlighted. *Right*: Comparison of the stem helix
1170 epitope conformation in the pre-fusion spike (*grey*), induced by CC40.8 binding (*orange*) and
1171 displayed on S2hlx-Ex19 (*magenta*).

1172

1173 **Figure 4**

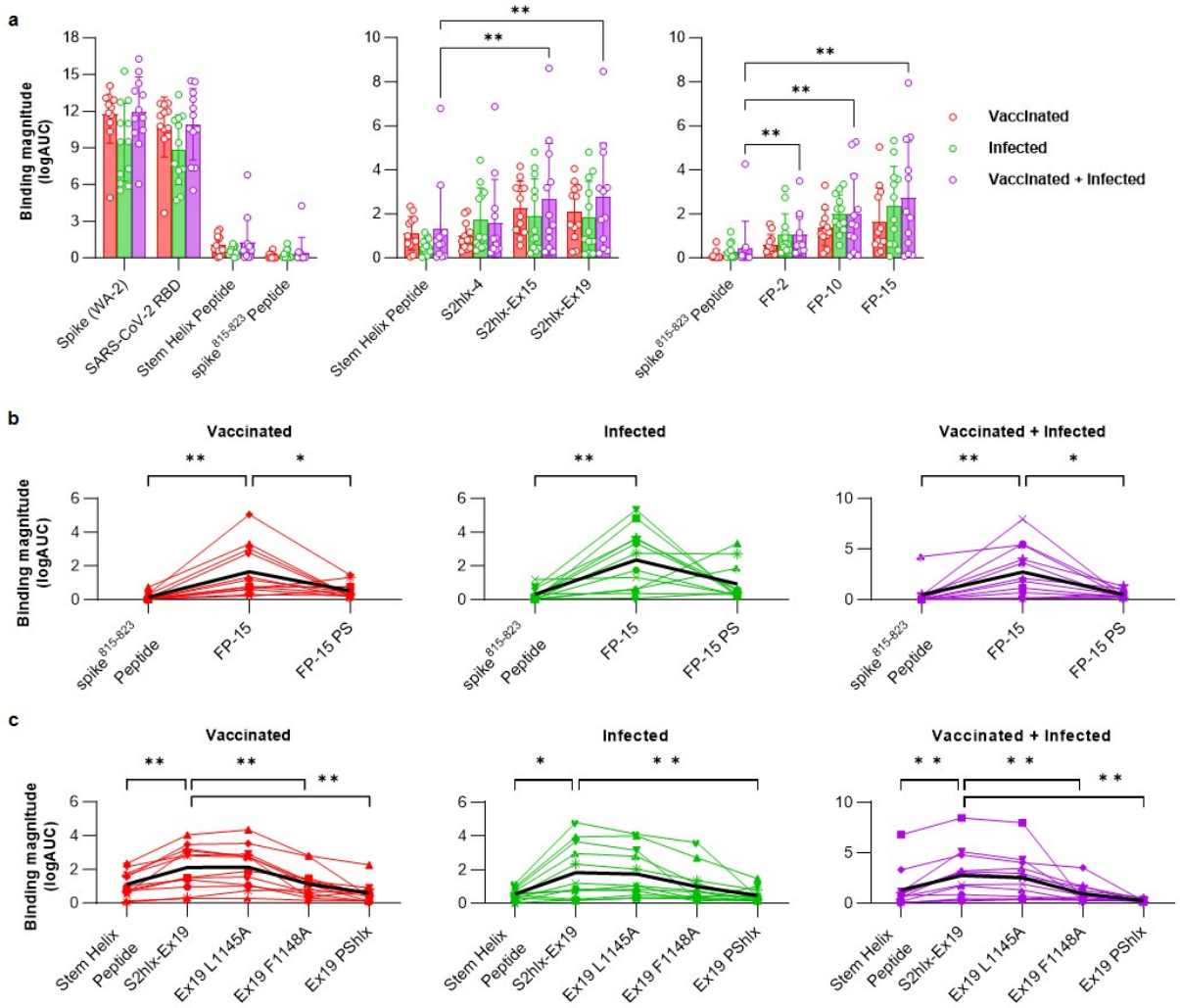

1174

1175 **Figure 4. Reactivity of engineered epitope scaffolds with sera from individuals with pre-**
1176 **existing immune responses to SARS-CoV-2 spike. (a)** *Left*: ELISA binding of sera or plasma
1177 from patients with pre-existing SARS-CoV-2 immunity acquired by vaccination (*red*), infection
1178 (*green*), or vaccination followed by infection (*purple*) to recombinant WA-2 spike and RBD or to
1179 synthetic peptides encoding the spike$^{815\text{-}823}$ peptide (residues 808-833) or the stem helix peptide
1180 (1140-1164). *Middle* and *right:* Binding of the same samples in **(a)** to select stem helix peptide

1181 and spike$^{815-823}$ peptide epitope scaffolds respectively. **(b)** Comparison between sera binding to
1182 the synthesized spike$^{815-823}$ peptide with FP-15 ES, and the parent scaffold from which FP-15 was
1183 derived and that lacks the grafted epitope (FP-15 PS). **(c)** Comparison between sera binding to
1184 the synthesized stem helix peptide with S2hlx-Ex19 ES, and with versions of this design where
1185 the epitope is mutated to reduce binding to either CC40.8 class antibodies (L1145A), to both
1186 CC40.8 and S2P6 classes of antibodies (F1148A), or where the epitope is replaced with the
1187 sequence from the parent scaffold it replaced (PShlx). Single lines represent measurements for
1188 individual samples in the respective cohort. For all graphs *=$p<0.05$ and **=$p<0.01$.

1189

1190 **Figure 5**

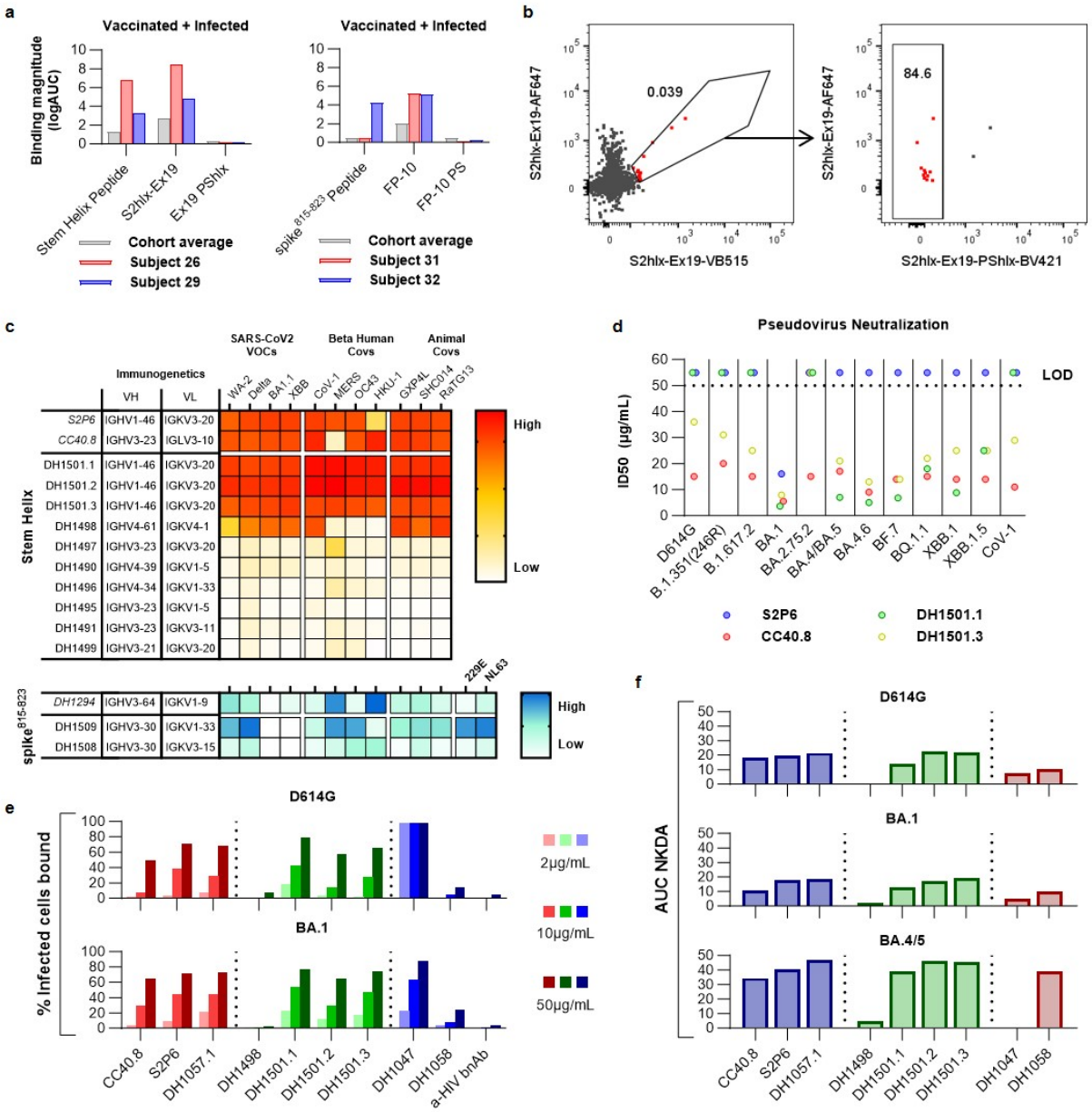

1191

1192 **Figure 5. Isolation and characterization of epitope scaffold reactive antibodies from**
1193 **subjects with pre-existing SARS-CoV-2 immunity. (a)** Sera binding profile of subjects from
1194 which B cells were isolated. Binding was measured to the synthetic peptide epitope, the epitope
1195 scaffold used as the sorting probe, and the corresponding parent scaffold (PS) that lacks the

1196 epitope and was employed for negative selection. **(b)** Representative FACS plots of memory B
1197 cells labeled with epitope scaffold probes. Cells from Subject 26 were labeled with S2hlx-Ex19
1198 conjugated to VB15 (x-axis) and AF647 (y-axis). A third bait comprising S2hlx-Ex19 PShlx
1199 conjugated to BV421 was used to exclude scaffold-specific memory B cells. **(c)** Binding of the
1200 isolated antibodies to diverse CoV spikes. **(d)** Neutralization of diverse pseudoviruses by isolated
1201 stem helix antibodies. **(e)** Binding of isolated antibodies to cells infected with different SARS-CoV-
1202 2 VOCs. Antibodies in *red* have been previously described, those depicted in *green* were isolated
1203 here, while those in *blue* represent controls; DH1047 targets the RBD domain; DH1058 targets
1204 the spike$^{815\text{-}823}$ peptide domain; anti-HIV antibody VRC01 was included as a negative control. **(d)**
1205 NK cell degranulation ability of mAbs from **(e)**.

1206

1207 **Figure 6**

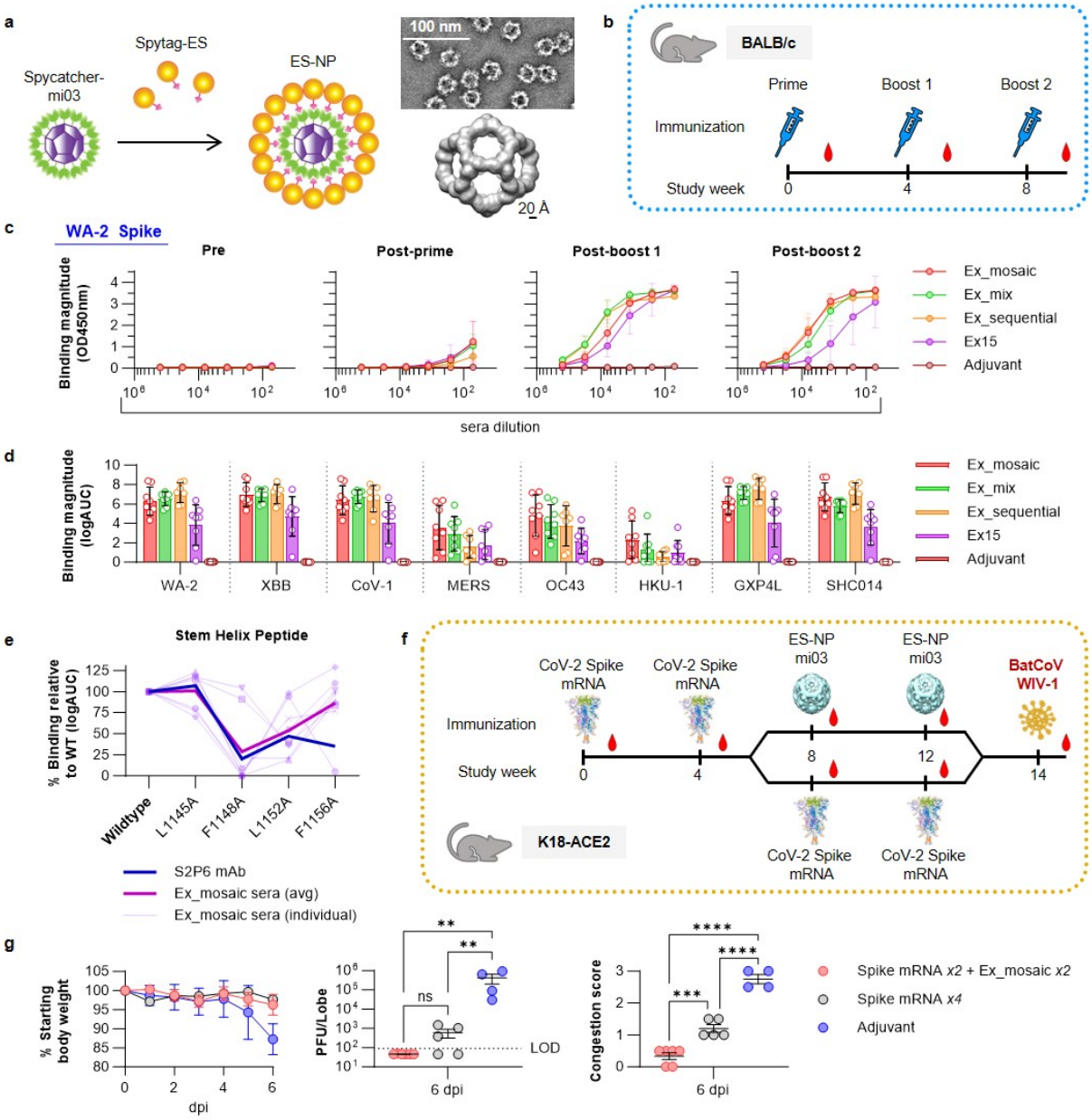

1208

1209 **Figure 6. Immunogenicity of stem helix epitope scaffolds. (a)** Development and NSEM
1210 analysis of the spycatcher/spytag mi03 nanoparticles displaying 60 epitope scaffold copies. **(b)**
1211 Study design to determine the immunogenicity of stem helix nanoparticles in BALB/c mice. **(c)**
1212 Binding of sera from animals immunized with the different epitope scaffold regimens against the

1213 WA-2 spike at different study time points. **(d)** Sera binding after the second boost against diverse
1214 CoV spikes. Values are calculated as the logarithm of the area under the curve for binding curves
1215 measured as in (c). **(e)** Binding of S2P6 mAb and sera from animals immunized with Ex_mosaic
1216 to the WT stem helix epitope peptide and mutated variants. **(f)** Study design to determine the
1217 protection ability of Ex_mosaic-NP against live coronavirus challenge. **(g)** Percentage weight loss
1218 in animals treated as in (f). Values represent the average per group, with error bars depicting the
1219 standard deviation. **(h)**. Lung congestion score and plaque analysis of infected animals. Data
1220 points correspond to individual animals. ns=not significant; **=p<0.01; ***=p<0.001 ****=p<0.0001

1221